SIAM J. APPL. MATH.
Vol. 50, No. 3, pp. 760-790, June 1990

008

BACK IN THE SADDLE AGAIN: A COMPUTER ASSISTED STUDY OF THE KURAMOTO–SIVASHINSKY EQUATION*

IOANNIS G. KEVREKIDIS†, BASIL NICOLAENKO‡§, AND JAMES C. SCOVEL‡

Abstract. A numerical and analytical study of the Kuramoto-Sivashinsky partial differential equation (PDE) in one spatial dimension with periodic boundary conditions is presented. The structure, stability, and bifurcation characteristics of steady state and time-dependent solutions of the PDE for values of the parameter α less than 40 are examined. The numerically observed primary and secondary bifurcations of steady states, as well as bifurcations to constant speed traveling waves (limit cycles), are analytically verified. Persistent homoclinic and heteroclinic saddle connections are observed and explained via the system symmetries and fixed point subspaces of appropriate isotropy subgroups of $O(2)$. Their effect on the system dynamics is discussed, and several tertiary bifurcations, observed numerically, are presented.

Key words. Kuramoto-Sivashinsky equation, bifurcation with symmetry, numerical bifurcation analysis, saddle connections

AMS(MOS) subject classifications. 35B32, 76E30, 58F14

1. Introduction.

The Kuramoto-Sivashinsky (K-S) equation

$$u_t + 4\Delta^2 u + \alpha(\Delta u + 1/2(\nabla u)^2) = 0 \tag{1.1}$$

arises as a model amplitude equation for interfacial instabilities in many physical contexts: Kuramoto and Tsuzuki (1976) derived it in the context of angular-phase turbulence for a system of reaction-diffusion equations modeling the Belousov-Zhabotinskii reaction in three space dimensions. Sivashinsky (1977) derived it to model small thermal diffusive instabilities in laminar flame fronts in two space dimensions. It has also been derived in the context of thin viscous film flow down vertical or inclined planes, interfacial instabilities between concurrent viscous fluids, or a fluid film with interfacial stress from adjacent gas flow, as well as in the context of drift waves in plasmas (Benney (1966), Nepomnyashschii (1973), Lin (1974), Cohen et al. (1976), Tsvelodub (1980), Shlang and Sivashinsky (1982), Alekseenko, Nakoryakov, and Pokusaev (1985), Chang ((1986a) and (1986b)). It is interesting to know that it can also be derived under scaling and symmetry arguments for cellular flows near a bifurcation (Fauve (1985)).

Both these physical systems and the K-S exhibit a wealth of spatially and temporally nontrivial dynamical behavior including chaos. The fact that it is a scalar equation makes it more tractable to numerical computation. Consequently, the K-S has been extensively used in the effort to understand and predict the complex dynamical behavior associated with these systems. It is a model example.

The systems modeled by the K-S exhibit weak interfacial turbulence characterized by coherent spatial structures (a small number of excited degrees of freedom) with

* Received by the editors November 16, 1987; accepted for publication (in revised form) February 21, 1989.

† Department of Chemical Engineering, Princeton University, Princeton, New Jersey 08544. The work of this author was supported by National Science Foundation grants EET-8717787 and CBT-8707090.

‡ Theoretical Division, Los Alamos National Laboratory, Los Alamos, New Mexico 87545.

§ The work of this author was partially supported by Air Force Office of Scientific Research grant R70-A. Department of Energy support through the hospitality of the Center for Nonlinear Studies, Los Alamos National Laboratory, Los Alamos, New Mexico is gratefully acknowledged.

complex temporal dynamics. This corroborates with the low-dimensionality of the global attractor of the K-S asserted by the Inertial Manifold Theorem of Nicolaenko, Scheurer, and Temam (1985), and Foias et al. (1987)).

In his original work Sivashinsky derived a more general amplitude equation, containing another parameter and an integral operator term, of which the equation we study is a special case (that of omitting the integral term). Thual, Frisch, and Hénon (1985) studied another special case (omitting the fourth-order term but retaining the integral operator) and used arguments based on a polar decomposition due to Lee and Chen (1982) to corroborate the low-dimensional behavior of their system.

In this paper we exploit detailed numerical stability and bifurcation information in order to provide directions for the analytic study and understanding of the complex K-S dynamics. We examine in detail the transitions to standing and rotating waves as well as the existence of persistent heteroclinic and homoclinic connections and their effect on the observable system dynamics. These connections (generically structurally unstable) appear structurally stable for reasons associated with the symmetries of the K-S. We will study the K-S in one spatial dimension. Although the physical relevance of periodic boundary conditions has been disputed and solutions on the entire line have been studied, we will use periodic boundary conditions because of the computational simplicity and also because of the interesting effect of the resulting rotational invariance on the system's bifurcations and saddle connections. In particular, our study may be considered a model case of bifurcations in the presence of the $O(2)$ symmetry group. The existence and stability of more complex bifurcations and/or saddle connections, due to the presence of symmetries, is also seen in Guckenheimer and Holmes (1986), Dangelmayr and Armbruster (1986), Guckenheimer (1986), and Aubry et al. (1986). Although this work is limited to primary and secondary (small α) phenomena, both our analysis and extant simulations point towards the persistence of such phenomena for higher values of the parameter α.

2. Motivation: the initial value problem. The K-S has been used as a prototype system to model the development of turbulence in physical systems. Its solutions are characterized by the coexistence of coherent spatial structures and temporal chaos. Extensive simulations of the initial value problem for the K-S have been performed by a number of researchers and have shown the existence of periodic cellular patterns (e.g., Michelson and Sivashinsky (1977), Michelson (1985), Hyman and Nicolaenko (1986), (1987), Hyman, Nicolaenko, and Zaleski (1985), Chen and Chang (1986), Frisch, She, and Thual (1986)). These simulations have also addressed the transitions in the dynamic behavior of the partial differential equation (PDE) as the spatial period of the patterns, i.e., the cell length, or our parameter α, grows. We have used two distinct numerical algorithms for the integration of the initial value problem. Both were variable step, variable order backward difference schemes, both integrating in Fourier space. The first algorithm (FTP, for Fast Fourier Transform Pseudospectral) written by Hyman, used a high-precision approximation to the spatial derivatives via FFT, while the second (GS) used a Galerkin true Spectral discretization, for which the appropriate set of ordinary differential equations (ODEs) was explicitly constructed in FORTRAN through the symbolic manipulator MACSYMA.

Our preliminary simulations yielded the following observations as α increases:

(1) For $\alpha < 4$, every set of initial conditions is attracted to the flat steady state solution $u_0 \equiv 0$. (See Fig. 2.1.)

(2) Between $\alpha = 4$ and $\alpha = 13.005$, transients get attracted to a nontrivial steady state. Because of the translational invariance of the differential equation restricted to

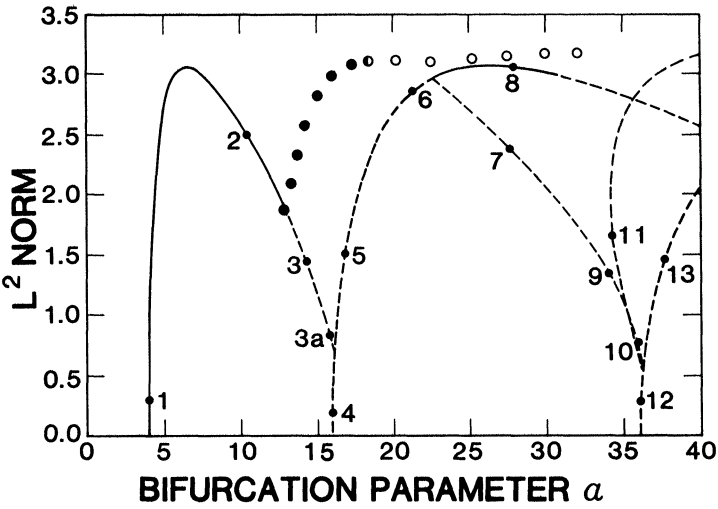

FIG. 2.1. *L^2 norm bifurcation diagram of the K-S for $0 < \alpha < 40$.* —— *Stable Steady States*; - - - - - *Unstable Steady States*; • • • • *Stable Rotating Waves*; ○○○○ *Unstable Rotating Waves. See Fig. 2.2 for representative waveforms sampled at points* $1, 2, \cdots 13$.

2π periodic functions, every translation of a steady state is also a steady state. This means that we have a one-parameter family of steady states, each of which is a shift of the others. Indeed, we observe that different transients are attracted to different members of this one-parameter family. For α near 4 these steady states are both small and qualitatively similar to $\cos(x)$, i.e., they go through one spatial oscillation between 0 and 2π (see Fig. 2.2, Points 1 and 4). We label this family of waves the *unimodal* steady states.

(3) Between $\alpha = 13.005$ and $\alpha = 17.399$, transients get attracted to a traveling wave solution, a function $u(x-ct)$ where c, the wave velocity, depends upon α. For each α we observe two waves, traveling in opposite directions. Due to the boundary conditions, each wave appears as a limit cycle, forming a closed curve in the phase space of the PDE. If we project this limit cycle on a plane of sine and cosine coefficients of any single Fourier mode, we obtain a circle (Fig. 2.3a). We label these solutions *rotating waves.*

(4) For values of α between 17.399 and 22.557, the observed long-term behavior consists of a pulsation between two states, which appear to be $\pi/2$-translations of each other, each state being invariant under π-translation. The transients linger close to one of these states for a comparatively long time before they pulse back to the other. Within the limits of our computational accuracy, the time spent near each state does not appear to progressively increase towards infinity; on the contrary, it appears to remain almost constant. The pulsation, projected on the $\cos(2x)$-$\sin(2x)$ coefficient plane ultimately appears as a straight line passing through the origin (Fig. 2.3b). Different pulsations, resulting from different initial conditions, when projected on this plane, give straight lines that are rotations of each other about the origin.

It is interesting to observe that these pulsations (which we label *the pulsing wave*) exist even for values of α below 17.399. We have observed them for values of α as low as 16.8. This means that for some interval below 17.399 the stable *rotating wave* solution coexists with a one-parameter family of stable *pulsing wave* solutions. Each type of wave has its own basin of attraction.

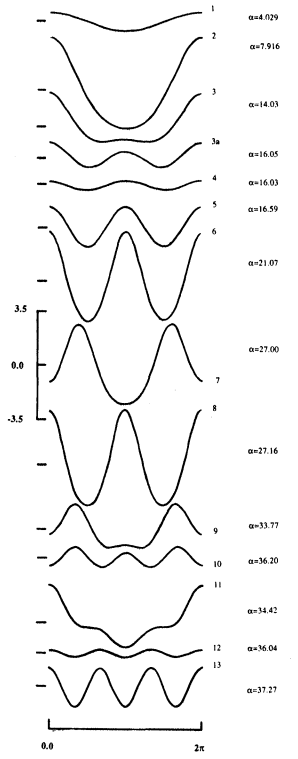

FIG. 2.2. *Steady state waveforms at representative points of the bifurcation diagram in Fig.* 2.1.

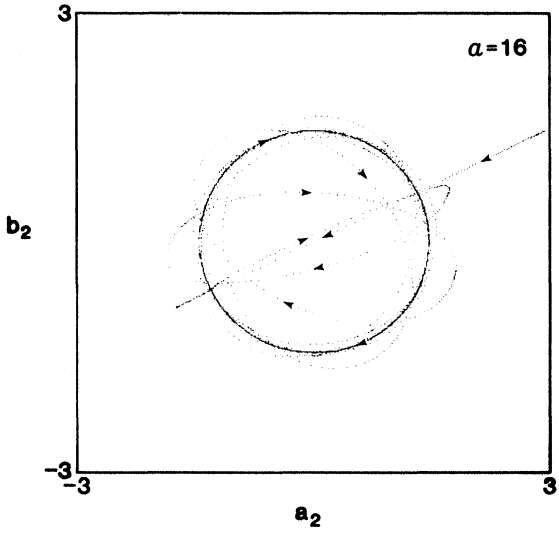

FIG. 2.3a. *Phase-plane projection of the transient approach to a stable rotating wave at* $\alpha = 16$.

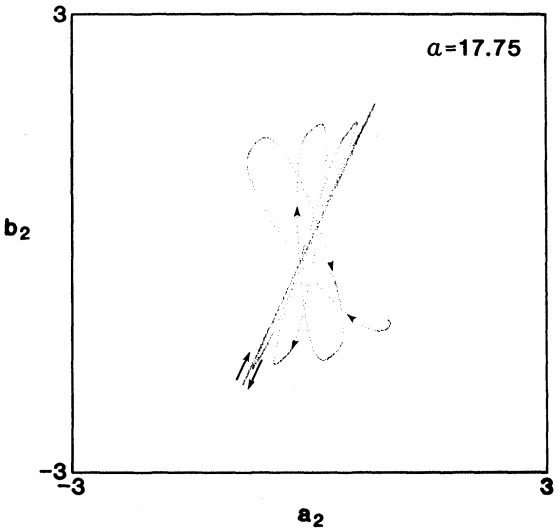

FIG. 2.3b. *Phase-plane projection of the transient approach to an attracting pulsing wave at* $\alpha = 17.75$.

(5) For values of α slightly larger than 22.557, the pulsing waves are not observed; a new family of attracting stable steady states appears instead, each of which is again a translation of the others. It is characteristic that these steady states do not appear to have any Fourier component in the odd modes. They actually appear two-humped close to $\alpha = 22.557$ (qualitatively similar to $\cos(2x)$), and for this reason we have labeled them *bimodal* steady states.

It is interesting to notice that qualitatively similar dynamics have been obtained by Aubry et al. (1986) for a low-dimensional dynamical system modeling the development of wall layer turbulence.

In what follows we attempt to analytically characterize the transitions giving birth to these various waveforms, which are persistently observed throughout the large-α regime.

3. Steady state bifurcations. We have normalized the K-S equation to an interval of length 2π; set the damping parameter to the original value derived by Sivashinsky, $\nu = 4$, and introduced the bifurcation parameter $\alpha = 4L^2$, where L is the size of a typical pattern scale. The equation can now be written as

$$\begin{aligned} &v_t + 4v_{xxxx} + \alpha[v_{xx} + \tfrac{1}{2}(v_x)^2] = 0, \\ &0 \leqq x \leqq 2\pi, \qquad v(x+2\pi, t) = v(x, t), \quad v(x, 0) = v_0(x). \end{aligned} \tag{3.1}$$

This equation is equivalent to (1.1) with a different time scaling. The mean value of the solution to this equation $m(t) = 1/2\pi \int_0^{2\pi} v(x, t)\, dx$ satisfies the drift equation

$$\frac{dm}{dt} = -\frac{\alpha}{4\pi} \int_0^{2\pi} v_x^2\, dx.$$

To normalize the drift to zero we solve for $u(x, t) = v(x, t) - m(t)$ which satisfies

$$u_t + 4u_{xxxx} + \alpha[u_{xx} + \tfrac{1}{2}(u_x^2)] + dm/dt = 0.$$

Let H^1 denote the space of 2π-periodic functions with one weak derivative in L^2, zero mean and inner product $\langle u, v \rangle = \int_0^{2\pi} u_x v_x\, dx$.

Consider the operator

$$F_\alpha(u) = -4u_{xxxx} - \alpha[u_{xx} + \tfrac{1}{2}(u_x^2) - \tfrac{1}{4\pi}\int_0^{2\pi} u_x^2].$$

Due to the even order spatial derivatives in the linear part of F as well as to the quadratic nonlinearity, there exists a number of linear subspaces of H^1 that are invariant under the flow of the K-S PDE

$$u_t - F_\alpha(u) = 0. \tag{3.2}$$

We refer to these as "invariant subspaces."

As we discussed above, the translational invariance of F generates one-parameter families of steady states and characterizes the rotating wave form. Restricting our attention to special invariant subspaces facilitates the analytic description of the steady state branches, their stability and the secondary bifurcations on them.

A technical comment is appropriate here. F, as well as G, as appears in § 4a, is not well defined on H^1 but must be redefined by the method of duality (see Berger (1978)). Let H^2 consist of the 2π-periodic functions with zero mean, two weak derivatives in L^2, and inner product $\langle u, v\rangle_2 = \int u_{xx}v_{xx}$. Then, we define a companion map to F, $\mathbb{F}$, by

$$\langle \mathbb{F}(u), v\rangle_2 = \int u_{xx}v_{xx} + \alpha\left[-\int u_x v_x + \tfrac{1}{2}u_x^2 v - \tfrac{1}{4\pi}\left(\int u_x^2\right)\int v\right]$$

for all $v \in H^2$. Then, $\mathbb{F}: H^2 \to H^2$ is differentiable, $d\mathbb{F}$ is Fredholm, index $= 0$, and all the machinery of the Implicit Function Theorem can be used. Integration by parts shows that solutions of $\mathbb{F}(u) = 0$ for $u \in H^2$ are weak solutions of $F(u) = 0$ and a classical regularity theorem shows that they are classical solutions. Note that for clarity this technical setting will not be referred to again (we work in L^2), but the apparently formal manipulations presented can be translated directly to the rigorous setting.

3a. Formalism: Projections and invariant subspaces. Actions of several important groups on the K-S are studied:

$O(2)$, the orthogonal group defined by the generators on the complex plane

$$\{z \to e^{i\theta}z,\ z \to \bar{z}\}, \qquad 0 \leqq \theta < 2\pi,$$

$Z(2)$, the group defined by the generator

$$\{z \to \bar{z}\},$$

$D(n)$, the dihedral subgroup of $O(2)$ defined by the generators

$$\{z \to e^{2\pi i/n}z,\ z \to \bar{z}\}.$$

We now introduce the formalism of projections we will employ in our bifurcation analysis. Define $Ru(x) = u(-x)$ and $Su(x) = u(x+\pi)$, the reflection and shift representations of $Z(2)$. Then, $R^2 = S^2 = I$, the identity, follows from the periodic boundary conditions and implies that

$$R_1 = (I+R)/2, \quad R_2 = (I-R)/2, \quad S_1 = (I+S)/2, \quad S_2 = (I-S)/2$$

are projections ($R_1^2 = R_1$, etc.). 2π-periodicity implies that

$$R_iS_j = S_jR_i, \quad i,j = 1,2.$$

Let $D = d(\cdot)/dx$. Then $RD = -DR$ and $SD = DS$ imply that

$$DR_1 = R_2D, \quad DR_2 = R_1D, \quad DS_1 = S_1D, \quad DS_2 = S_2D$$

with the consequence that $D^2 \equiv D \cdot D$ and $D^4 \equiv D \cdot D \cdot D \cdot D$ both commute with all R's and S's.

The identity $I = R_1S_1 + R_1S_2 + R_2S_1 + R_2S_2$ provides an orthogonal decomposition of H^1 into the ranges of these four projections, henceforth labeled with the names of the corresponding projection, i.e., $H^1 = R_1S_1 \oplus R_1S_2 \oplus R_2S_1 \oplus R_2S_2$. Note that R_1S_1 is the space of even, π-periodic functions, R_1S_2 the even, π-antiperiodic functions, R_2S_1 the odd, π-periodic functions, and R_2S_2 the odd, π-antiperiodic functions.

We decompose F into its action on these four subspaces, the only nontrivial terms being the nonlinearity. To compute this, we need to know the following product rules, easily derived from $R^2 = S^2 = I$, $R(ab) = Ra \cdot Rb$ and $S(ab) = Sa \cdot Sb$.

$$R_1(ab) = R_1a \cdot R_1b + R_2a \cdot R_2b,$$

$$R_2(ab) = R_1a \cdot R_2b + R_2a \cdot R_1b,$$

$$S_1(ab) = S_1a \cdot S_1b + S_2a \cdot S_2b,$$

$$S_2(ab) = S_1a \cdot S_2b + S_2a \cdot S_1b.$$

Note also that $(R_1S_1)\ 1 = 1$ while $(R_1S_2)\ 1 = (R_2S_1)\ 1 = (R_2S_2)\ 1 = 0$.

The product rules and differentiation rules lead directly to the following:

$$R_1S_1\left[(Du)^2 - \frac{1}{2\pi}\int_0^{2\pi}(Du)^2\right]$$
$$= (DR_1S_1u)^2 + (DR_2S_1u)^2 + (DR_1S_2u)^2 + (DR_2S_2u)^2$$
$$- \frac{1}{2\pi}\int_0^{2\pi}[(DR_1S_1u)^2 + (DR_2S_1u)^2 + (DR_1S_2u)^2 + (DR_2S_2u)^2]$$

$$R_1S_2\left[(Du)^2 - \frac{1}{2\pi}\int_0^{2\pi}(Du)^2\right] = 2[DR_2S_1u \cdot DR_2S_2u + DR_1S_1u \cdot DR_1S_2u]$$

$$R_2S_1\left[(Du)^2 - \frac{1}{2\pi}\int_0^{2\pi}(Du)^2\right] = 2[DR_2S_1u \cdot DR_1S_1u + DR_2S_2u \cdot DR_1S_2u]$$

$$R_2S_2\left[(Du)^2 - \frac{1}{2\pi}\int_0^{2\pi}(Du)^2\right] = 2[DR_2S_1u \cdot DR_1S_2u + DR_1S_1u \cdot DR_2S_2u].$$

Four invariant subspaces are apparent from this decomposition. They are

$$R_1S_1,$$

$$R_1S_1 \oplus R_2S_1 = S_1 \ (\pi\text{-periodic functions}),$$

$$R_1S_1 \oplus R_1S_2 = R_1 \ (\text{even functions}),$$

$$R_1S_1 \oplus R_2S_2 \equiv L.$$

Note that they consist of R_1S_1 and direct sums of R_1S_1 and each of the other three subspaces formed by the projections. This situation is schematically shown in Fig. 3.1.

The above invariant subspaces are fixed sets of isotropy subgroups of the fundamental group $O(2)$ acting upon the K-S equation, and the K-S flow is equivariant under these isotropy subgroups. Recall that the isotropy subgroup of a subspace W contained in H^1 is the subgroup Σ^W of $O(2)$ defined by the condition that, for every σ in Σ^W and w in W, $\sigma(w) = w$. The fixed set W^* of a subgroup Σ^W of $O(2)$ is the subspace $W^* \supseteq W$ such that, for every σ in Σ^W and w in W^*, $\sigma(w) = w$. $O(2)$ is the space of orthogonal transformations of the complex plane. Consider a function u in

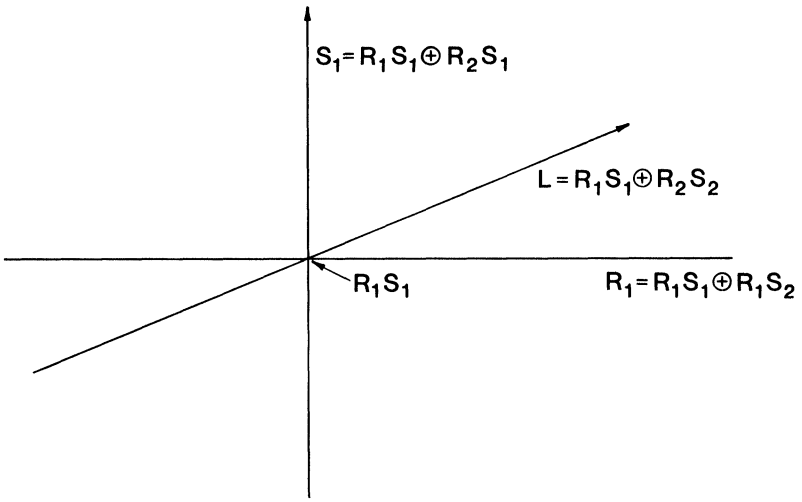

FIG. 3.1. *Schematic of the direct sum structure of the invariant subspaces produced by the four projections* R_1S_1, R_1S_2, R_2S_1, R_2S_2.

H^1 as a function on the unit circle in the complex plane. Then the action of an element g in $O(2)$ on u is defined by $g^*(u) = u \circ g$.

The four invariant subspaces above are fixed sets of isotropy subgroups of $O(2)$. In particular:

R_1S_1 is the fixed set of $D(2)$;

S_1 is the fixed set of the group whose generator is the π-rotation;

R_1 is the fixed set of the group $Z(2)$;

L is the fixed set of the group whose generator is reflection about the imaginary axis.

Each constitutes a different representation of $Z(2)$.

3b. Primary branches and scaling properties. For the rest of the paper, all integration limits will be assumed to be between 0 and 2π.

The trivial branch $u_0 = 0$. For $\alpha < 4$ the only steady state is $u_0 \equiv 0$. This can be seen as follows: $0 = \int F_\alpha(u) u_{xx} = 4\int (u_{xxx})^2 - \alpha \int (u_{xx})^2$ where $\int u_x^2 u_{xx} = 0$ by periodicity. Poincaré's inequality $\int (u_{xxx})^2 \geqq \int (u_{xx})^2$ then gives $0 \geqq (4-\alpha)\int (u_{xx})^2 \geqq 0$ with the result that u is identically zero. Since the image of any ball about the origin under the flow is eventually contained in a pre-compact subset (Foias et al. (1987)) the flow must come arbitrarily close to u_0 and, because u_0 is linearly stable, the flow must terminate there. Therefore, u_0 is the global attractor for $\alpha < 4$.

The restriction lemma. Under the decomposition $I = R_1 + R_2$ the nonlinear terms $(Du)^2 - (1/2\pi)\int (Du)^2$ decouple as follows:

$$R_1\{(Du)^2 - (1/2\pi)\int (Du)^2\} = |DR_1u|^2 + |DR_2u|^2 - (1/2\pi)\int (|DR_1u|^2 + |DR_2u|^2)$$

$$R_2\{(Du)^2 - (1/2\pi)\int (Du)^2\} = 2(DR_1u \cdot DR_2u).$$

A quick inspection shows that R_1 is an invariant subspace. Let $H_n \subseteq H$ denote the subspace of even $2\pi/n$ periodic functions. H_n is an invariant subspace of F. $H_1 (= R_1)$ and H_n are fixed sets of the isotropy subgroups $D(n)$. $dF(0) = -4D^4 - \alpha D^2$ has

eigenvalues $\lambda_k = \alpha k^2 - 4k^4$ with eigenfunctions $\cos(kx)$ and $\sin(kx)$. At $\alpha = \alpha_0 = 4$ for *fixed* k, the two-dimensional kernel span $\{\cos(kx), \sin(kx)\}$ becomes the on dimensional kernel span $\{\cos(kx)\}$ when F is restricted to the invariant subspace H

Classical equivariant bifurcation theorems (Golubitsky and Schaeffer, 1985) ensu the existence of *at least one* bifurcation branch in H_k.

RESTRICTION LEMMA. *For α near $4k^2$ the entire bifurcation of solutions to $F_\alpha(u) =$ lies in H_k.*

Proof. To emphasize the dependence of F upon the parameter α we will oft write $F(u, \alpha)$ instead of $F_\alpha(u)$. Let $e = \cos(kx)$ and $\sigma = \sin(kx)$ be a basis for tl kernel of $dF(0) = -4D^4 - \alpha_0 D^2$. Let $u \in \{e, \sigma\}^\perp$ and consider the Liapunov-Schmi reduction

$$P_e F(t_1 e + t_2 \sigma + u, \alpha) = 0,$$
$$P_\sigma F(t_1 e + t_2 \sigma + u, \alpha) = 0,$$
$$CP_{e,\sigma} F(t_1 e + t_2 \sigma + u, \alpha) = 0,$$

where $P_e u = \langle e, u \rangle$, $P_\sigma u = \langle \sigma, u \rangle$ and $CP_{e,\sigma} u = u - e \cdot P_e u - \sigma \cdot P_\sigma u$. Since $t_1 e + t_2 \sigma$ $\tau(\cos(kx + \theta))$ where $\tau = (t_1^2 + t_2^2)^{1/2}$, $\sin\theta = t_1/\tau$ and $\cos\theta = t_2/\tau$, and since F invariant under θ-shifts, and a θ-shift of u remains orthogonal to e and σ, we can ju as well solve $F(\tau e + u, \alpha) = 0$ with u orthogonal to e and σ. The decomposition appea as follows:

$$P_e F(\tau e + u, \alpha) = 0, \tag{3.3}$$
$$P_\sigma F(\tau e + u, \alpha) = 0, \tag{3.4}$$
$$CP_{e,\sigma} F(\dot{\tau} e + u, \alpha) = 0. \tag{3.5}$$

Equation (3.5) is solved for a unique $u(\tau, \alpha)$ by the Implicit Function Theorem reduci the search for steady state solutions to two bifurcation equations

$$f_1(\tau, \alpha) = P_e F(\tau e + u(\tau, \alpha), \alpha) = 0$$
$$f_2(\tau, \alpha) = P_\sigma F(\tau e + u(\tau, \alpha), \alpha) = 0.$$

Now consider the same problem in the restricted subspace H_k. The system solve is

$$P_e F(\tau e + w, \alpha) = 0 \tag{3.6}$$
$$CP_e F(\tau e + w, \alpha) = 0 \quad \text{in } H_k \tag{3.7}$$

with w orthogonal to e and in H_k. Equation (3.7) is solved for a unique $w(\tau, \alpha)$ the Implicit Function Theorem, with the resulting bifurcation equation being

$$g_1(\tau, \alpha) = P_e F(\tau e + w(\tau, \alpha), \alpha) = 0.$$

Because $F(H_k) \in H_k$, solutions to (3.7) are also solutions to (3.5). By uniquene $w(\tau, \alpha) = u(\tau, \alpha)$ and $f_2(\tau, \alpha) \equiv 0$ since σ is odd. Also $f_1(\tau, \alpha) \equiv g_1(\tau, \alpha)$, giving identic solutions. The proof is finished. □

The unimodal branch U. By the restriction lemma, near $\alpha = 4$, we can restrict the bifurcation equations to $H_1 = R_1$.

THEOREM. *The bifurcation of steady state solutions from $u_0 \equiv 0$ at $\alpha = 4$ is a pitchfork bifurcation.*

Proof. The bifurcation equation is $f(\tau, \alpha) = P_e F(\tau e + u(\tau, \alpha), \alpha)$ where $u(\tau, \alpha)$ is the unique solution to $CP_e F(\tau e + u(\tau, \alpha), \alpha) = 0$. Let $\alpha_0 = 4$ and denote all partial derivatives evaluated at $\tau = 0$, $\alpha = \alpha_0$ by f_τ, $f_{\tau\alpha}$, and u_τ, etc. We need to verify the pitchfork conditions $0 = f_\tau = f_{\tau\tau} = f_\alpha$ with $f_{\tau\tau\tau} \neq 0$ and $f_{\tau\alpha} \neq 0$ (Golubitsky and Schaeffer (1985)).

Since e is orthogonal to the range of dF,

$$f_\tau = P_e dF(e + u_\tau) = 0 \text{ and } f_\alpha = P_e dF u_\alpha + P_e \partial_\alpha F(0) = P_e dF u_\alpha = 0.$$

Differentiating $d/d\tau\ (CP_e F) = 0$ indicates that $u_\tau = 0$. Thus,

$$f_{\tau\alpha} = P_e \partial_\alpha dF(e) = -\int e e_{xx} = \int e_x^2 = \pi$$

and

$$f_{\tau\tau\tau} = 3 \int e e_x (u_{\tau\tau})_x;$$

where

$$dF u_{\tau\tau} = -CP_e d^2 F(e, e),$$

which can be written as

$$(-4D^4 - 4D^2) u_{\tau\tau} = e_x^2 - (1/2\pi) \int e_x^2 = \sin^2 x - 1/2 = -(1/2) \cos 2x,$$

and has the solution

$$u_{\tau\tau} = (1/96) \cos 2x.$$

Consequently, $f_{\tau\tau\tau} = -(1/8) \int \cos^2(x) \sin^2(x) < 0$. Finally, the condition $f_{\tau\tau} = 0$ is a consequence of the fact that f is an odd function of τ. This can be seen as follows. Let Π denote the π-shift. Since $-e = \Pi e$, the unique solution of $CP_e F(-\tau e + u(-\tau, \alpha), \alpha) = 0$ is $u(-\tau, \alpha) = \Pi u(\tau, \alpha)$. Therefore,

$$\begin{aligned}
f(-\tau, \alpha) &= \int eF(-\tau e + u(-\tau, \alpha), \alpha) \\
&= \int eF(\Pi(\tau e + u(\tau, \alpha), \alpha)) \\
&= \int e\Pi F(\tau e + u(\tau, \alpha), \alpha) \qquad (F \text{ commutes with } \Pi) \\
&= -\int \Pi e \Pi F(\tau e + u(\tau, \alpha), \alpha) \\
&= -\int eF(\tau e + u(\tau, \alpha), \alpha) \\
&= -f(\tau, \alpha).
\end{aligned}$$

The proof is finished. □

We label the branch of steady state solutions bifurcating from the trivial solution at $\alpha = 4$ the *unimodal* branch U.

The k-modal branch K. We define the k-fold replication of a function $u \in H$ by $(R_k u)(x) = u(kx)$. Note that if $u \in H_1$, then $R_k u \in H_k$. Also note that if $v \in H_k$, R_k^{-1} defined by $(R_k^{-1} v) \equiv v(x/k)$ determines a map from H_k to H_1. The chain rule implies that

$$F_{k^2\alpha}(R_k u) = R_k F_\alpha(u) \quad \text{or}$$

$$R_k^{-1} F_\alpha(w) = F_{\alpha/k^2}(R_k^{-1} w) \quad \text{for } w \text{ in } H_k,$$

so that if u is a solution of $F_\alpha(u) = 0$ then $w = R_k u$ is a solution of $F_{\alpha k^2}(w) = 0$. For α near $4k^2$ the restriction lemma shows that the bifurcating solutions lie entirely in H_k, the fixed set of $D(k)$. The gist of this is that if w is in H_k and is on K, the k-modal solutions bifurcating from $u_0 \equiv 0$ at $\alpha = 4k^2$ then $R_k^{-1} w$ is a solution bifurcating from $R_k^{-1} u_0 \equiv 0$ at $\alpha = 4k^2/k^2 = 4$, that is, it is part of the unimodal branch. Therefore, $R_k : U \to K$ is an isomorphism with the conclusion that the bifurcation at $\alpha = 4k^2$ is pitchfork, and the solutions are just k-fold replications of elements of U, which we label the *k-modal* branch K.

A series of secondary bifurcations connects these branches rendering their unambiguous labeling impossible; we will therefore reserve the term k-modal branch to indicate that portion of the branch bifurcating at $\alpha = 4k^2$ that remains in H_k. By the previous discussion, each such branch will initially lie in H_k and is therefore part of the k-modal branch.

The bimodal branch B and the trimodal branch T. The bifurcations described in this paper involve primarily the unimodal branch U $(k = 1)$, the bimodal branch B $(k = 2)$, and the trimodal branch T $(k = 3)$, bifurcating, respectively, at $\alpha = 4$, $\alpha = 4 \times 2^2 = 16$, and $\alpha = 4 \times 3^2 = 36$. The bimodal branch B lies in H_2 and consists entirely of two-fold replications of elements of U while the trimodal branch T lies in H_3 and consists entirely of three-fold replications of elements of U.

3c. Secondary bifurcations from the primary branches. It is well known (e.g., Chen and Chang, (1986)) that the primary branches are involved in an intricate web of secondary bifurcations occurring away from the trivial solution. In an effort to detect, classify and analyze these secondary bifurcations, we numerically followed the primary branches via continuation.

We used numerical contraction mapping techniques (Newton-Raphson and continuation methods) to locate the steady states of a 16- and 32-mode Galerkin pseudospectral discretization of the PDE. Since every shift of a steady state solution is also a solution, the linearization around any steady state will possess a zero eigenvalue, whose eigenvector points in the direction of translational invariance in Fourier space. To remove this singularity and obtain convergence of the Newton-Raphson, we singled out one particular element of this one-parameter family. This can be accomplished by pinning any single Fourier coefficient to a prescribed value. An alternative method follows from the observation that the projection of this one-parameter family onto the kth mode coefficient plane $\{a_k, b_k\}$ is a circle. Thus, we can simply prescribe $\arctan(b_k/a_k)$, which is equivalent to choosing a specific representation of $O(2)$.

Another way of eliminating the one-parameter family of solutions is to restrict the computations to one of the invariant subspaces we discussed above, for example R_1, the space of even functions (only cosines in the Fourier expansion) or $L = R_1 S_1 \oplus R_2 S_2$ (even mode cosines and odd mode sines in the Fourier expansion). With such a

modification, it is possible to use one of the standard continuation/bifurcation codes, like AUTO written by Doedel (1981). It is important to keep in mind that the global attractor inherits the same symmetries and the same isotropy subgroups. If the computations are restricted to any of the isotropy subgroups discussed above (under which the K-S flow is equivariant) the stability characteristics of the located solution can (and will, as shown below) be affected by such a restriction. Specifically, different elements of the same branch of steady states can and do have stable and unstable manifolds in different invariant subspaces. Therefore on restricted subspaces solutions related by a simple translation can undergo distinctly different bifurcation sequences (see for example, Chen and Chang (1986)).

In the full Fourier space, upon convergence of the Newton-Raphson, the spectrum of the full Jacobian is computed. We locate the secondary bifurcations by observing the trajectories of the rest of the spectrum of the Fréchet derivative dF as α varies. We have observed several occasions in which a second eigenvalue, not always the least stable, crosses the imaginary axis through zero with nonzero speed. We have distinguished these bifurcations by observing the relation of the critical eigenvector (corresponding to the eigenvalue crossing zero) with the neutral eigenvector (pointing in the direction of the translational invariance) as well as through observations of the modes contributing to the critical eigenvector. We now describe the numerical spectrum at representative points on the bifurcation diagram (Fig. 3.2).

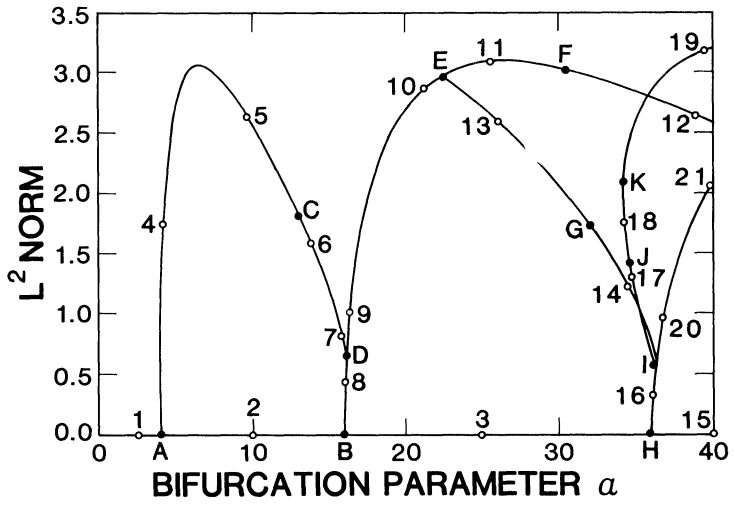

FIG. 3.2. *Steady state bifurcation diagram. Capital letters indicate the location of bifurcation points. The spectrum of the linearization around these points as well as around representative points indicated with roman numerals is displayed in Fig.* 3.3.

For $\alpha < 4$ (point 1 in Fig. 3.2) the spectrum of the linearization around the zero solution consists of sets of double eigenvalues on the negative real axis (Fig. 3.3a). We will name these sets of eigenvalues "first pair" and "second pair" counting from right to left on the real axis. At $\alpha = 4$ (point A) the first pair reaches 0 (Fig. 3.3b). For $\alpha > 4$ (point 2), this pair crosses zero to the right-hand plane for the linearization around the zero branch (Fig. 3.3c). For the unimodal branch (point 4) this pair splits; one eigenvalue (corresponding to translational invariance) stays pinned at zero, while the other recedes back on the negative real axis (Fig. 3.3d). All other pairs split in a similar fashion, initially remaining on the negative real axis.

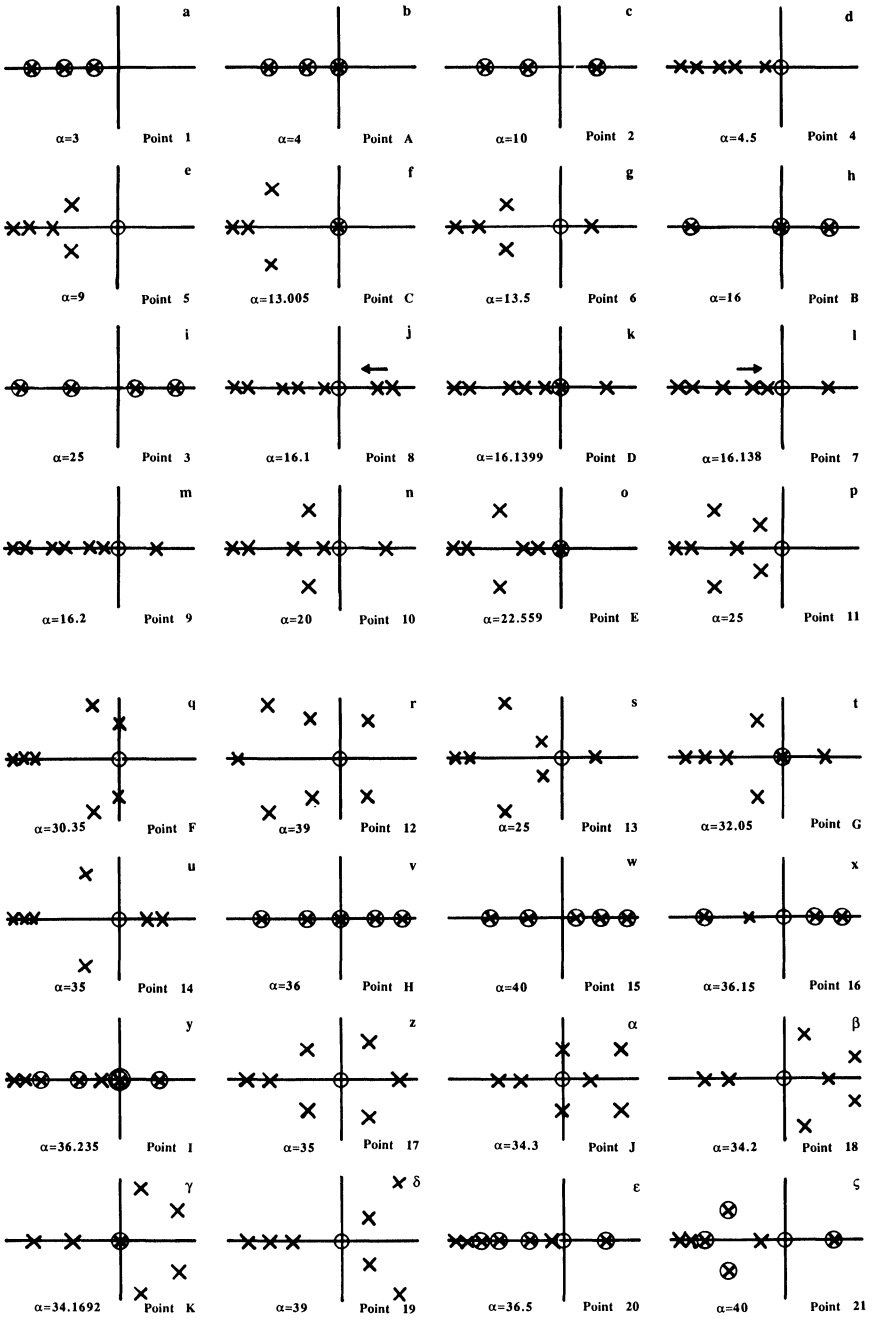

FIG. 3.3a-z. *Schematic of the eigenvalue structure of the linearization around representative steady states of Fig.* 3.2. ×: *simple eigenvalue*; ⊗: *double eigenvalue*; ⊛: *triple eigenvalue*; ○: *the eigenvalue corresponding to the translational invariance.*

As we move further on the unimodal branch (point 5) the rightmost eigenvalue of the second pair approaches the receding eigenvalue of the first pair. They collide and split into complex conjugates with negative real part, rendering the transient approach to the stable steady state oscillatory (Fig. 3.3e). This leaves the real axis

open for the remaining real eigenvalue of the second pair to cross through zero (point C) to the positive real axis (point 6) with nonzero speed, at $\alpha = 13.005$ (see Figs. 3.3f and 3.3g). We observe that as α approaches the bifurcation value 13.005 from below, the eigenvector of the critical eigenvalue tends to align itself with the neutral eigenvector indicating that, at that point, the zero eigenvalue has algebraic multiplicity two but geometric multiplicity one. The steady state loses stability (point C) to a pair of attracting rotating waves. Our observations of the spectrum are instrumental in our analysis of this symmetry breaking bifurcation.

We now return to the already unstable trivial solution (point 2). At $\alpha = 2^2 \times 4 = 16$, the second pair reaches zero (point B) and it crosses to the right hand plane (point 3) for the trivial branch (Figs. 3.3h and 3.3i). One new nontrivial branch of steady states (the bimodal branch B) is born at 16. As we discussed above, it is a scaled replica of U. The critical (second) pair will again split on this branch: one eigenvalue will remain at zero, while the other will recede on the real axis to the left-hand plane; all other eigenvalue pairs will similarly split on the real axis. The fundamental difference between U and B is that B does not contain any odd mode (S_2) components, since it belongs to the fixed set of $D(2)$. It also inherits the instability of the trivial solution: it has a two-dimensional unstable manifold (point 8), corresponding to the two positive real eigenvalues from the splitting of the first pair (Fig. 3.3j).

At $\alpha = 16.1399$ (point D, Fig. 3.3k) the unimodal branch U and the bimodal branch B merge in a pitchfork bifurcation. This occurs as the leftmost eigenvalue of the first pair approaches zero from positive values on the bimodal branch (Fig. 3.3j) while the rightmost eigenvalue of the third pair approaches zero from negative values on the unimodal branch. Notice that close to point D the two complex conjugate eigenvalues of the linearization on U have become real again (point 7, Fig. 3.3l). The bimodal branch gains one degree of stability on its way towards becoming an attractor. For $\alpha > 16.1399$ (point 9) it has a one-dimensional unstable manifold (Fig. 3.3m.) We will discuss this bifurcation (which is invisible to simple simulations, since both branches participating are unstable) in more detail in § 5. It is interesting to observe that, as the unimodal branch approaches point D, its odd-mode (S_2) components shrink to zero. In addition, its eigenvectors approach the corresponding eigenvectors of the bimodal branch which have special modal structure. They live in either R_1S_1 (the fixed set of $D(2)$), or in R_1S_2, R_2S_1, or R_2S_2 which are complementary to R_1S_1 in the remaining three invariant subspaces. This is a consequence of the fact that $dF(u)$ with $u \in R_1S_1$ commutes with the four projections, and so the spectrum and eigenvectors split accordingly.

As we further increase α (point 10) the leftmost eigenvalue of the second pair and the rightmost one of the third pair merge and become complex (Fig. 3.3n). At $\alpha = 22.559$ (point E) the last remaining unstable eigenvalue of the bimodal branch approaches zero on the real axis and crosses it towards negative values (Fig. 3.3o). This renders the bimodal branch stable (point 11 and Fig. 3.3p). This bifurcation is distinguished from the rotating wave bifurcation at point C in that the critical eigenvector remains orthogonal to the neutral eigenvector throughout the crossing. This symmetry breaking bifurcation gives birth to a new steady state branch which we label the *bi-tri BT* branch since it will later connect with the trimodal branch at $\alpha = 36.235$ (point I). We return to the bimodal branch. At point 11 the least stable eigenvalues are a complex conjugate pair. At $\alpha = 30.35$ this pair reaches the imaginary axis in a Hopf bifurcation giving birth to an oscillatory (but not rotating wave) periodic solution (point F, Fig. 3.3q). The complex conjugate pair then crosses into the right-hand plane (point 12, Fig. 3.3r).

Returning to point E, we follow the newborn BT branch which has components in all modes and has initially one positive eigenvalue (point 13, Fig. 3.3s). At $\alpha = 32.05$ (point G) the first negative eigenvalue crosses zero with nonzero speed towards the right-hand plane, while the geometric multiplicity of the double zero eigenvalue is one (Fig. 3.3t). In this sense it resembles the bifurcation at $\alpha = 13.005$ where a rotating wave bifurcated from the unimodal branch. We therefore expect a similar symmetry breaking bifurcation here. After this bifurcation (point 14) the BT branch has two positive real eigenvalues (Fig. 3.3u) on its way to colliding with the trimodal branch.

At $\alpha = 4 \times 3^2 = 36$ (point H) the third pair of eigenvalues of the trivial solution comes to zero (Fig. 3.3v) and crosses to the right-hand plane (point 15, Fig. 3.3w). This signals the birth (in a pitchfork bifurcation) of the trimodal branch T (invariant under $D(3)$, point 16, Fig. 3.3x); this branch inherits four positive eigenvalues from the trivial solution and, similarly to the unimodal and bimodal branches, its critical pair splits. One eigenvalue of this pair remains at zero (corresponding to the translational invariance) while the second one recedes into the left-hand plane. It is interesting to observe that not all remaining pairs split on this trimodal branch. The first and second (right-hand plane) pairs as well as the fourth and fifth (left-hand plane) pairs to the left of the split third pair remain double. This is a consequence of the fact that since the trimodal steady state u is invariant under the shift $Tu(x) = u(x + 2\pi/3)$, both v and Tv are eigenvectors with the same eigenvalue and in these cases v and Tv are distinct.

At $\alpha = 36.235$ (point I, Fig. 3.3y) the trimodal branch collides with the BT branch, as a double eigenvalue from the right-hand plane crosses to the left-hand plane. This means that at point I we momentarily have a triple eigenvalue at zero. We are currently investigating the effect of group symmetries in the unfolding of this bifurcation, using spectral information from the BT branch which merges there with T. The trimodal branch gains two degrees of stability on its way toward becoming an attractor (point 20, Fig. 3.3ε). The double eigenvalue that crossed at point I passes through a simple eigenvalue, merges with the next double eigenvalue in an algebraic multiplicity four eigenvalue, which then splits into a double complex conjugate pair (point 21, Fig. 3.3ς).

After the BT branch hits the T branch at point I, it continues toward smaller values of α. At $\alpha = 35$ (point 17, Fig. 3.3z) it has three positive eigenvalues, two of which are complex conjugate. The least stable eigenvalue in the left-hand plane is a complex conjugate pair. As we further decrease α, this pair crosses the imaginary axis in a Hopf bifurcation ($\alpha = 34.3$, point J, Fig. 3.3α) into the right-hand plane (point 18, Fig. 3.3β). The real positive eigenvalue recedes then in a turning point bifurcation ($\alpha = 34.1692$, point K, Fig. 3.3γ) into the left-hand plane (point 19, Fig. 3.3δ) as now α increases along the BT branch.

The simple bifurcation diagram of Fig. 2.1, where we plot the L^2 norm of the solution versus α, does not do justice to several important geometric characteristics of the bifurcation structure. To illuminate this structure we have constructed three-dimensional bifurcation diagrams in which the L^2 norm and one selected Fourier component of the solution (or two selected Fourier components of the solution) are plotted versus α. Figure 3.4 illustrates the collision of the unimodal branch U with the bimodal branch B. Both Fig. 3.4a and Fig. 3.4b have been obtained by restricting the equation to the space of even functions (R_1). For this reason, they possess certain asymmetries; Two representatives of U in R_1 emerge at point A, and terminate in a pitchfork at D. These two branches have the same L^2 norm but opposite odd cosine coefficients. Therefore they appear as two distinct branches in Fig. 3.4b and as a single branch in Fig. 3.4a. At point D they collide with one of the two representatives of B

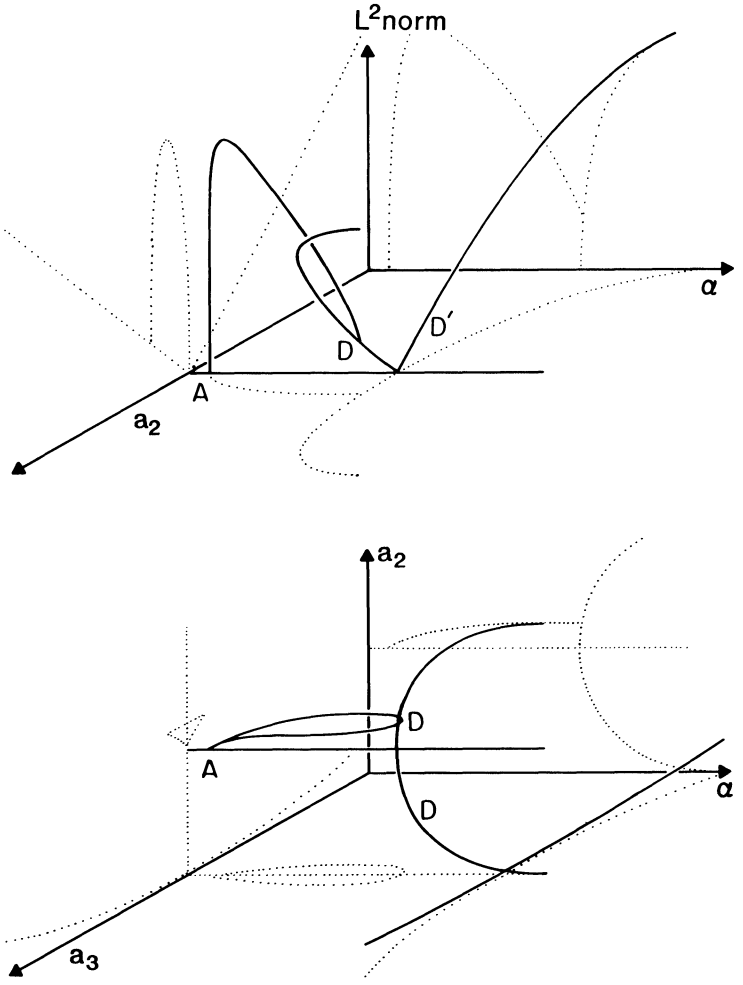

FIG. 3.4a, b. *Three-dimensional bifurcation diagram restricted to even functions, elucidating the merging of the unimodal and bimodal branches. The broken lines are the projections onto the corresponding planes. The projection onto the* α-L^2 *norm plane in Fig.* 3.4a *coincides with the norm bifurcation diagram in Fig.* 3.2. *Under the restriction to even functions, two distinct representatives of the bimodal branch (each a* $\pi/2$ *shift of the other) appear, and project onto the same curve in the* α-L^2 *norm plane. However, the unimodal branch merges with only one representative of the bimodal branch, and this asymmetry is lost under this projection. Similarly, the bifurcation diagram* 3.4b *illustrates the two representatives of the unimodal branch which were indistinguishable with the choice of axes in Fig.* 3.4a.

in R_1. The second representative (D') of B in R_1 has its weak unstable eigendirection orthogonal to R_1 and, as a result, *does not undergo a bifurcation in* R_1. On the other hand, it is this second representative D' of the bimodal branch in R_1 that bifurcates to the BT branch at E', while the original bimodal D *does not undergo this secondary bifurcation in* R_1 at E.

Figure 3.5 illustrates the connection of the bimodal and the trimodal branch via the BT branch. Similar to the above discussion, the two representatives (E' and E, Fig. 3.5a) of the bimodal branch B in R_1 have the same L^2 norm and will appear as one single branch in Fig. 3.5b. Two representatives of BT (F and F') bifurcate in R_1 from the bimodal branch at E'. Each of them hits a representative of the trimodal branch T in R_1 at F and F', respectively. They both undergo a further turning point

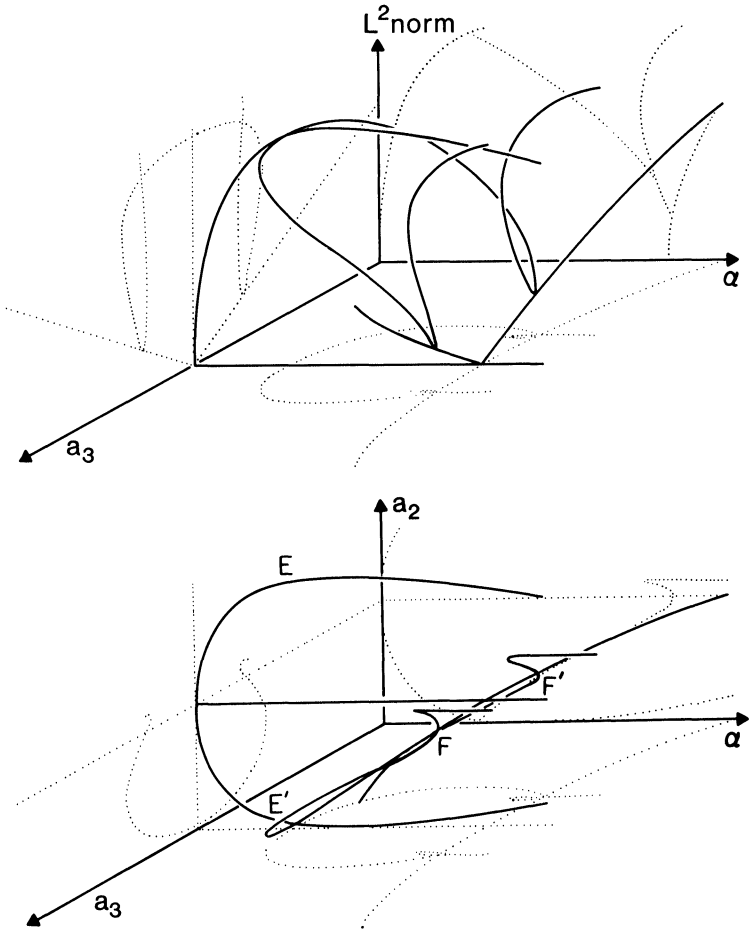

FIG. 3.5a, b. *Three dimensional bifurcation diagram restricted to even functions, elucidating the connection of the bimodal branch with the trimodal branch via the bi-tri branch. Broken lines are the projections onto the corresponding planes. Again, the projection onto the* α-L^2 *norm plane in Fig.* 3.5a *coincides with part of the norm bifurcation diagram in Fig.* 3.2. *Under the restriction to even functions there are two representatives of both the trimodal and the bi-tri branch visible in Fig.* 3.5a, *but the choice of axes in Fig.* 3.5b *is necessary in order to distinguish the two representatives of the bimodal branch, of which one gives birth to the bi-tri branch.*

bifurcation simultaneously (H and H'), and continue toward larger values of α. We will investigate these and further bifurcations in a later publication.

Figure 3.6 combines Fig. 3.4a and 3.5a showing the unimodal, bimodal and trimodal branches and the branches connecting them in R_1 for $\alpha < 40$.

4. The rotating waves. As mentioned in § 3c, at $\alpha = 13.005$ the linearization about each unimodal steady state has an eigenvalue at zero with algebraic multiplicity two but with geometric multiplicity one. As α crosses 13.005, the eigenvalue splits. One remains at zero, while the other crosses into the right-hand plane rendering the steady states unstable (saddles with a one-dimensional unstable manifold). The attractor now is a stable *rotating wave*: a constant shape waveform, moving with constant velocity in the direction of translational invariance. These rotating waves bifurcate from the unimodal branch: initially, the waveform approximates that of a steady state (see Fig. 4.1) while the wavespeed is zero at $\alpha = 13.005$ and increases continuously thereafter. Two such rotating waves coexist, one of them an exact reflection about $x = 0$ and

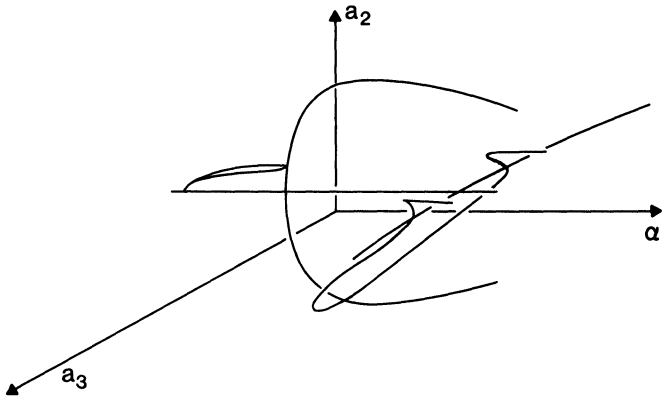

FIG. 3.6. *The full bifurcation diagram for* α *between* 0 *and* 40, *restricted to even functions. The projections have been omitted for clarity.*

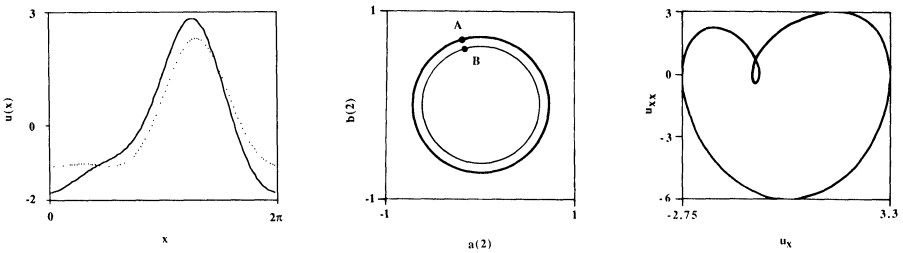

FIG. 4.1. *An instantaneous snapshot* (*Fig.* 4.1a, *solid line*) *of the clockwise rotating wave whose projection is point A in Fig.* 4.1b. *For comparison, we superimpose the nearby* (*unstable, dotted line*) *steady state whose projection is point B in Fig.* 4.1b. *The arrows indicate the direction of rotation. There also exists a clockwise rotating wave whose waveform is a reflection of the counterclockwise rotating wave. These waves are limit cycles both for the* PDE *and for a set of* ODEs *in the waveframe coordinate* $\xi = x - ct$, *where c is the wave velocity. Their phase plane projections appear therefore as closed curves in both frames* (*Fig.* 4.1b *for the* PDE *and Fig.* 4.1c *for the* ODE).

traveling with opposite velocity of the other. Trajectories initialized on a local approximation of the unstable manifold of the unimodal states will be attracted to these two waves: one side of the unstable manifold will be attracted to the clockwise rotating wave, while the antipodal side will be attracted to the counterclockwise rotating one.

4a. The bifurcation theorem. Since the geometric dimension of the null space does not increase, we cannot have a classical steady state bifurcation at $\alpha = 13.005$. In the context of Couette-Taylor flow, Iooss (1984), Chossat (1985), and Chossat and Iooss (1985), have shown that the equivariant symmetry breaking yields a rotating wave. Their proof is essentially a local normal form analysis on the center manifold. Here we provide a new geometric proof of this result for the Kuramoto-Sivashinsky equation.

We seek rotating wave solutions, namely $w(x - ct)$ which satisfies $w_t - F_\alpha(w) = 0$. We label $\alpha = 13.005\ (=)\ \beta$.

At the bifurcation point $\alpha = \beta$ we let u_0 be the unimodal state at criticality, $F_\beta(u_0) = 0$. At the critical value 13.005, the eigenvector of the double zero eigenvalue corresponds to translational invariance of F, namely, differentiating F with respect to x gives $dF_\beta(u)\ u_x = 0$. We label

$$e \equiv \frac{du_0}{dx}$$

and let σ be the generalized eigenvector defined by

$$dF_\beta(u_0)\sigma = e.$$

From now on, restricting the operators to functions with null mean, we label

$$dF_\beta(u_0) \equiv L_0.$$

The latter is a Fredholm operator of index zero, and its adjoint also possesses a double zero eigenvalue with

$$L_0^* e^* = 0, \quad L_0^* \sigma^* = e^*.$$

The above implies the orthogonality condition

$$\langle e^*, e\rangle = 0 \tag{4.1}$$

which in turn allows the following normalizations:

$$\begin{aligned} &\langle e^*, \sigma\rangle = 1, \\ &\langle \sigma^*, e\rangle = 1, \\ &\langle \sigma, \sigma^*\rangle = 0. \end{aligned} \tag{4.2}$$

(Replace σ (σ^*) by appropriate linear combinations of σ and e, (σ^* and e^*).)

Following ideas from Iooss (1984) we construct a center manifold at $\alpha = \beta$, *equivariant under the group* $O(2)$. Let us decompose w as follows:

$$w = \tau_s[u_0 + A\sigma + Z(\alpha, A)] \tag{4.3}$$

where A is a real amplitude, τ_s the shift operator $x \to x + s$ and Z describes a center manifold which contains in fact the whole circle of solutions $\{\tau_s u_0,\ s \in \mathbf{T}^1\}$, with

$$Z(0,0) = 0 \qquad \frac{\partial Z}{\partial \alpha}(0,0) = \frac{\partial Z}{\partial A}(0,0) = 0.$$

Since

$$\begin{aligned} &Re = -e, \text{ that is } R_2 e = e \text{ and} \\ &R\sigma = -\sigma, \text{ that is } R_2 \sigma = \sigma, \end{aligned}$$

the equivariance propagation leads to

$$\begin{aligned} \frac{ds}{dt} &= A + h(\alpha, A) \\ \frac{dA}{dt} &= f(\alpha, A) \end{aligned} \tag{4.4}$$

where functions h and f are $O(A)$ and odd in A, that is

$$f(\alpha, A) = a_1(\alpha - \beta)A + a_3 A^3 + \cdots.$$

The reduced system (4.4) on the center manifold is not truncated and results only from the equivariance. Clearly, solutions $\pm A_0$ where

$$A_0^2 = -\frac{a_1(\alpha - \beta)}{a_3} \tag{4.5}$$

correspond to rotating waves with velocities

$$\begin{aligned} &\omega_\pm = \pm A_0 + h(\alpha, \pm A_0) \text{ and} \\ &\omega_+ = -\omega_-. \end{aligned} \tag{4.6}$$

We need only compute a_1 and a_3 to know the direction of the bifurcation and the stability of these rotating waves.

The lowest order approximation to the center manifold. We explicitly construct the lowest order approximation to (4.4) to $O(\varepsilon^3)$, setting $\alpha-\beta=\varepsilon^2$, and remarking that $A=O(\varepsilon)$. In {4.3} we label

$$A\sigma+Z(\alpha, A)\equiv\tilde{u}. \tag{4.7}$$

The K-S equation $w_t+F_\alpha(w)=0$ can be rewritten as:

$$\frac{ds}{dt}\tau_s e+\frac{ds}{dt}\tau_s\nabla\tilde{u}+\frac{\partial\tilde{w}}{\partial t}+N(\tilde{w})=L_0\tilde{w} \tag{4.8}$$

where

$$\tilde{w}=\tau_s\tilde{u}=A\tau_s\sigma+\tau_s Z(\alpha, A) \tag{4.9}$$

and

$$N(\tilde{w})=(\alpha-\beta)N_1(\tilde{w})+\beta N_2(\tilde{w}) \tag{4.10a}$$

with

$$\begin{aligned} N_1(\tilde{w})&=\tilde{w}_{xx}+\frac{1}{2}(\tilde{w}_x)^2-\frac{1}{2L}\int_0^L(\tilde{w}_x)^2dx\\ N_2(\tilde{w})&=\frac{1}{2}(\tilde{w}_x)^2-\frac{1}{2L}\int_0^L(\tilde{w}_x)^2\,dx. \end{aligned} \tag{4.10b}$$

We establish the following lemma, which is needed for the proper application of Fredholm's alternative to L_0.

LEMMA 4.1. *Let Z be orthogonal to both e^* and σ^*. Specifically, $Z\in P_0\mathbf{H}$, where*

$$P_0\equiv I-\langle e^*, \rangle\sigma-\langle\sigma^*, \rangle e. \tag{4.11}$$

Then L_0 is an isomorphism on $P_0\mathbf{H}$, that is, $L_0Z=g$, $g\in P_0\mathbf{H}$ admits a unique solution.

Proof. Use the biorthogonality conditions (4.1), (4.2). For Z orthogonal to both e^* and σ^* note that:

$$\langle L_0Z, e^*\rangle=0$$

$$\langle L_0Z, \sigma^*\rangle=\langle Z, e^*\rangle=0.$$

Remark. From $\tilde{u}=A\sigma+Z$ we have $A=\langle\tilde{u}, e^*\rangle$, and $\langle\tilde{u}, \sigma^*\rangle=0$ provided that $P_0Z=Z$. From now on we restrict Z to the subspace $P_0\mathbf{H}$.

We now can explicitly construct the system (4.4). We systematically use the biorthogonality conditions (4.1), (4.2). First, take the scalar product of (4.8) with $\tau_s\sigma^*$ and *factor out the shift operator* τ_s (everything commutes with τ_s):

$$\frac{ds}{dt}=\{A-(\alpha-\beta)\langle\sigma^*, N_1(A\sigma+Z)\rangle-\beta\langle\sigma^*, N_2(A\sigma+Z)\rangle\}\{1+\langle\sigma^*, \nabla Z\rangle\}^{-1}. \tag{4.12}$$

Here we have used in an essential way that

$$\langle L_0\tilde{u}, \sigma^*\rangle\equiv\langle\tilde{u}, e^*\rangle\equiv\langle A\sigma, e^*\rangle\equiv A$$

$$\langle\sigma^*, \nabla\sigma\rangle=0 \quad (\text{since } R_2\sigma^*=\sigma^*, R_2\nabla\sigma=0).$$

To establish the second equation in system (4.4), take the scalar product of (4.8) with

$\tau_s e^*$ and factor out the shift operator

$$\frac{dA}{dt} = -\left\{(\alpha-\beta)\langle e^*, N_1(A\sigma+Z)\rangle + \beta\langle e^*, N_2(A\sigma+Z)\rangle + \frac{ds}{dt}\langle e^*, \nabla Z\rangle\right\} \tag{4.13}$$

with ds/dt given by (4.12) where we used the biorthogonality conditions (4.1)-(4.2) and $\langle e^*, \nabla\sigma\rangle = 0$ (since $R_2 e^* = e^*$ and $R_2\nabla\sigma = 0$).

To construct the lowest order approximation $O(\varepsilon^3)$ to {4.12}, {4.13} we set

$$Z = A^2 Z_2 + \text{h.o.t.}$$

This we must verify by considering the equation for Z obtained by projecting (4.8) with $\tau_s P_0$ and factoring out τ_s:

$$Z = L_0^{-1}\left\{(\alpha-\beta)P_0 N_1(A\sigma+Z) + \beta P_0 N_2(A\sigma+Z) + \frac{ds}{dt}P_0(A\nabla\sigma+\nabla Z) + \frac{dA}{dt}\frac{\partial Z}{\partial A}\right\} \tag{4.14}$$

where ds/dt and dA/dt are given by (4.12) and (4.13).

To lowest order

$$\frac{ds}{dt} = A + \text{h.o.t.} \quad \text{and} \quad \frac{dA}{dt} = a_1\varepsilon^2 A + b_1 A^3 + \text{h.o.t.}$$

Hence,

$$Z = A^2 L_0^{-1}\left\{\beta\left(\frac{1}{2}(\nabla\sigma)^2 - \frac{1}{2L}\int_0^L (\nabla\sigma)^2 dx + \nabla\sigma\right\} + \text{h.o.t.}\right.$$

(4.15) and

$$Z_2 = L_0^{-1}\left\{\beta\left(\frac{1}{2}(\nabla\sigma)^2 - \frac{1}{2L}\int_0^L (\nabla\sigma)^2\, dx + \nabla\sigma\right\}.\right.$$

Here we used:

$$P_0(\nabla\sigma)^2 = (\nabla\sigma)^2 \text{ and } P_0(\nabla\sigma) = (\nabla\sigma) \text{ since } R_2\nabla\sigma = 0.$$

Finally, expanding (4.12)-(4.13) we obtain the lowest order approximations:

$$\frac{ds}{dt} = A - (\alpha-\beta)A\langle\sigma^*, \sigma_{xx}\rangle - \beta A^3\langle\sigma^*, \nabla\sigma\nabla Z_2\rangle - A^3\langle\sigma^*, \nabla Z_2\rangle \tag{4.16}$$

$$\frac{dA}{dt} = -(\alpha-\beta)A\langle e^*, \sigma_{xx}\rangle - \beta A^3\langle e^*, \nabla\sigma\nabla Z_2\rangle - A^3\langle e^*, \nabla Z_2\rangle. \tag{4.17}$$

We verify numerically that $a_1 = -\langle e^*, \sigma_{xx}\rangle \neq 0$. □

4b. Computation and numerical stability of the rotating waves. The asymptotic shape of the waveform and the stability of the rotating wave close to the bifurcation were obtained in the previous section. In order to track the branch of rotating waves away from the bifurcation point and to accurately locate and characterize their subsequent (tertiary) bifurcations, it is necessary to resort to numerical computations.

The rotating wave, due to the periodicity imposed by the boundary conditions, appears as a limit cycle of the full PDE. The wave will also appear as a limit cycle in the wave frame ODE

$$c(dw/d\xi) + F_\alpha(w) = 0.$$

In the first case (full PDE) we obtain this limit cycle and its period T by solving a two point free boundary value problem through a contraction mapping (Newton-Raphson). The integration of the variational equations, necessary for this formulation, was performed by a modified third-order semi-implicit Runge-Kutta scheme with step control. After each integration step for the system equations, the LU-decomposed Jacobian was saved so that the variational integrations required only backsubstitutions. Upon convergence, the characteristic (Floquet) multipliers were available and provided the quantitative linearized stability of the located periodic trajectory.

We performed these computations for 16 and 32 mode Galerkin pseudospectral discretizations of the PDE. In both cases, four of the 16 or 32 multipliers were effectively nonzero. Two of them were complex conjugates and we followed them on the rotating wave branch as a function of α. The results are shown in Fig. 4.2 in which we observe that at $\alpha = 17.399$ they exit the unit circle in the complex plane at $\theta \approx 145°$. No supercritical attractor is observed numerically, and we therefore believe that this is a subcritical bifurcation; further investigation is necessary to elucidate this phenomenon and its interaction with the system symmetries.

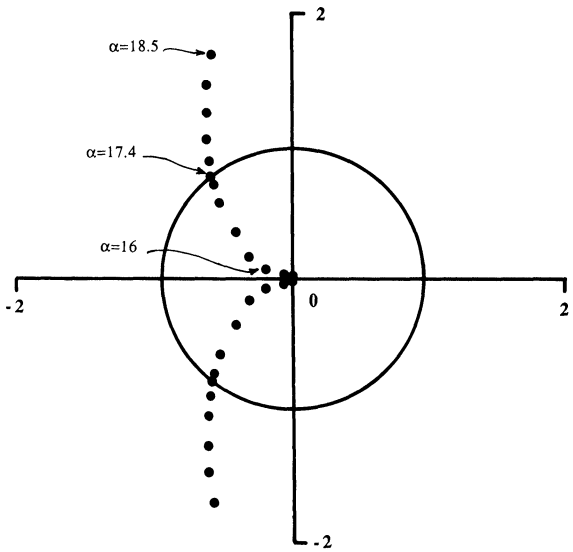

FIG. 4.2. *Variation of the principal Floquet multipliers of the rotating wave as α varies. At $\alpha = 17.399$ a pair of complex conjugate multipliers crosses the unit circle at an angle $\theta \approx 145°$, and the rotating wave loses stability, probably to a subcritical torus.*

Locating the same limit cycles in the ODE wave frame is an easier task computationally: this is a system of three coupled nonlinear ODEs, derived from (2.2). Problems associated with the drift of our integrated form of the K-S and numerical tricks for removing this drift in the wave frame are discussed in detail in another publication (Kevrekidis, Hyman, and Nicolaenko (in preparation)). The most important characteristic of this work is that, due to the existence of the drift, the stability of the limit cycle in the wave frame does not correspond to the stability of the rotating wave for the full PDE. The drift term, appearing as a parameter in the above system of three ODEs, is really a nonlocal integral term depending upon the solution u over the full period 0 to 2π. Perturbations of the limit cycle in the wave frame will necessarily affect this integral term; the Floquet multipliers of this limit cycle, which describe the fate of small perturbations for *constant* drift, do not therefore correspond to true perturba-

tions in the PDE. This problem is absent in our wave computations in the full Fourier space.

5. The saddle connections. Our numerical observations of "pulsing waves" as described in § 2, as well as reports of "bouncy" states in other numerical experiments (Cohen et al. (1976), Chen and Chang (1986), Hooper and Grimshaw (1985)) strongly suggest the existence of saddle-type states, as well as some form of homoclinic connections. We confirmed that the relatively quiescent parts of the transients for values of α between approximately 16.8 and 22.557 had spatial profiles numerically indistinguishable from our bimodal steady states. The two quiescent states between which the transients alternate are $\pi/2$-shifts of each other. This led to a numerical and analytical investigation of the unstable manifolds of these saddles and of the relation of the $\pi/2$-shift, the action of the subgroup $D(4)$, with the projections we defined earlier. In the following sections we will provide sound numerical and analytical evidence for the existence and persistence of said homoclinic and heteroclinic connections within and across families of steady states.

5a. Homoclinic loops and the pulsing wave. In a typical numerical experiment (Fig. 5.1a, $\alpha = 18.00$), two bimodal steady states u and u', each being a $\pi/2$-translation of the other, were located through a Newton-Raphson solution of the steady state equations. Upon convergence of the Newton iteration, the eigenvalues and corresponding eigenvectors of the linearization were computed numerically. Each saddle-type state had a single unstable direction (from the single positive eigenvalue of the Jacobian). We approximate locally the unstable manifold $W^u(u)$ by taking a small segment on each side (uB and $u\Gamma$) of the unstable eigenvector (higher order local approximations of the unstable manifold are also possible). We initialize a trajectory at the point B which approximates a point on $W^u(u)$, and integrate the Galerkin true spectral discretization forward in time. We observe that this trajectory quickly becomes attracted to the *unstable* $\pi/2$-shifted bimodal steady state u'. The actual solution shape during this transient is shown in Fig. 5.1b. The same is true for a transient initialized on the point Γ approximately lying on the other side of $W^u(u)$. We now perform a similar computation for the point u'. Trajectories initialized approximately on both sides of $W^u(u')$ (points B' and Γ') quickly become attracted to the original point u, a $\pi/2$-shift of u'. Note that u, like u' is an *unstable* steady state.

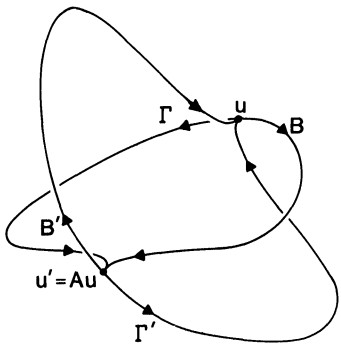

FIG. 5.1a. *A perturbation along the unstable manifold Γ or B of the bimodal steady state u tends to the diametrically opposed steady state $u' = Au$ (the $\pi/2$ shift of u). Likewise, a perturbation along the unstable manifold Γ' or B' of the bimodal steady state u' tends to $u = Au'$.*

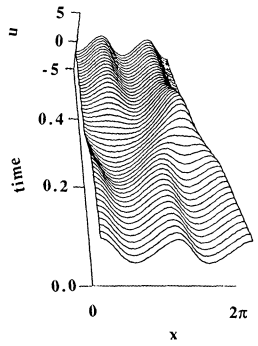

FIG. 5.1b. *Illustration of the solution shape during the transition from the neighborhood of one bimodal steady state to the neighborhood of its $\pi/2$ shift.*

If the FFT-based integrator is used, the trajectories emanating from our special initial conditions are initially very close to the ones we described above; their long-term behavior however is strikingly different: as the transient approaches a saddle-type solution, its component in the unstable eigendirection of the saddle grows sufficiently to eventually throw the trajectory off in the direction of this unstable manifold. Traveling in this unstable direction, the trajectory approaches the vicinity of the diametrically opposed saddle, the $\pi/2$ shift of the initial one, inducing this sequence to be repeated indefinitely.

The startling discrepancy in the qualitative dynamics strongly suggest that, while both integrators have truncation errors, the Galerkin-based discretization appears to respect some symmetry or invariance of the full K-S equation. A Galerkin truncation up to mode n will indeed possess the same invariant subspaces as the full equation restricted to the first n Fourier modes. This motivated the following analysis of the relation between the unstable eigendirections, the $\pi/2$-shift and the invariant subspaces of § 3a.

Let A, the generator of $D(4)$ restricted to R_1 be defined by $Au(x) = u(x+\pi/2)$. The following identities hold:

$$AR_2S_2 = R_1S_2A,$$

$$AR_1S_2 = R_2S_2A,$$

$$AR_1S_1 = R_1S_1A,$$

$$AR_2S_1 = R_2S_1A.$$

We can then compute the effect of A on the invariant subspaces.

$$AR_1S_1u = R_1S_1Au \Rightarrow A: R_1S_1 \to R_1S_1,$$

$$A(R_1S_1u + R_2S_1u) = R_1S_1Au + R_2S_1Au \Rightarrow A: S_1 \to S_1,$$

$$A(R_1S_1u + R_1S_2u) = R_1S_1Au + R_2S_2Au \in L \Rightarrow A: R_1 \to L,$$

$$A(R_1S_1u + R_2S_2u) = R_1S_1Au + R_1S_2Au \in R_1 \Rightarrow A: L \to R_1.$$

The first two results are immediate consequences of the $D(4)$ action on the fixed sets of the appropriate isotropy subgroup. The last two are more significant. The space L is the fixed set of the isotropy subgroup defined by reflection with respect to the imaginary axis. The action of $D(4)$ sends it to the fixed set of $Z(2)$ defined by complex conjugation. Conversely, the action of $D(4)$ sends R_1 to L.

The two points on the bimodal branch consist of a point u and its $\pi/2$ shift Au, with u in R_1S_1 (see § 3b). Since R_1S_1 is invariant under A, Au is also in R_1S_1. u can be chosen (between u and Au) so that it has one unstable eigendirection $v \in R_2S_2$. Now consider the invariant subspace $L = R_1S_1 \oplus R_2S_2$. $u \in R_1S_1$ and $v \in R_2S_2$ implies that $u + v \in L$, but the unstable eigendirection at Au is

$$Av = AR_2S_2v = R_1S_2Av \in R_1S_2$$

which is H^1 and L^2 orthogonal to L with the consequence that Au is a sink when the flow is restricted to L.

The numerical evidence that

(a) u is a saddle in L, while Au is a *sink* in L;

(b) trajectories starting approximately on the unstable manifold of u are attracted to Au;

(c) probably no other steady states than u and Au exist in L combined with the analytical evidence that

(a′) u is a saddle in L while Au is an attractor in L;

(b′) $L \supset W^u(u)$;

(c′) $L \perp W^u(Au)$,

indicates that the connection observed in the Galerkin approximation integration is a genuine characteristic of the full K-S flow. This structure is illustrated schematically in Fig. 5.2. It can be seen there that two loops exist constrained to the subspaces R_1 and L_1, respectively, each of which consists of two distinct saddle connections. Since this structure involves two elements of the bimodal branch, we call it a *homoclinic* loop.

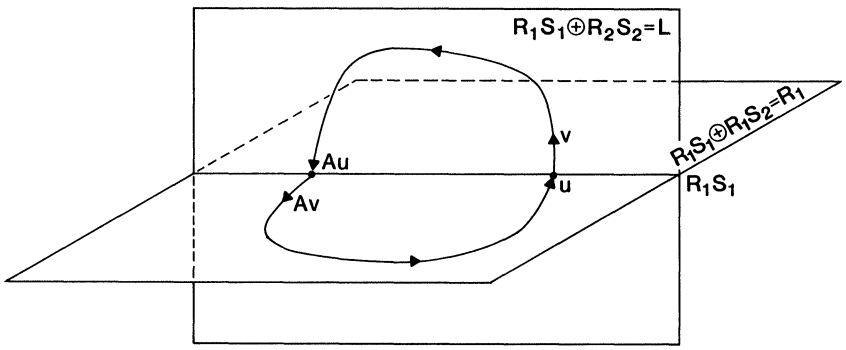

FIG. 5.2. *A perturbation in the unstable direction v of the unstable bimodal fixed point u remains in the invariant subspace L and tends to the bimodal steady state Au, which appears as a sink, since its unstable direction Av is orthogonal to L.*

Warning. Working in R_1, where two distinct representatives of the bimodal branch exist and are connected by their unstable manifolds, heteroclinic might seem the more natural term. However, we consider homoclinic a more appropriate characterization of the connection between a steady state and its images under studied symmetry groups, since these images possess the same modal structure.

Similar considerations to the above hold if we interchange u and Au and replace L with R_1. It is amusing—and rather fortunate—that any magnitude perturbation of u in the unstable eigendirection seems to be attracted to Au for the GS integration. This is a consequence of the fact that the invariant subspaces are linear, and the truncated Galerkin true spectral discretization commutes with projection onto these four subspaces.

It is important to mention that, while the homoclinic loop exists for the entire interval between $\alpha = 16.1399$ and 22.557, it is only attracting for α greater than approximately 16.8. As a matter of fact, even after it becomes attracting, and until the rotating wave loses stability at $\alpha = 17.399$, the homoclinic loop coexists with it and each has its own basin of attraction. For $\alpha > 17.399$ the homoclinic loop seems to be the only attractor until $\alpha = 22.557$, when the single positive eigenvalue of the linearization around the saddle bimodal states crosses through zero to the negative real axis. This kills the unstable eigendirection of the bimodal steady states leaving them stable and causing the annihilation of the homoclinic loop.

The coexistence of the rotating wave as an attractor with an attracting homoclinic loop necessitates some saddle-type object whose stable manifold will provide the boundary between the basins of attraction of the stable solutions. The fact that no supercritical stable torus appears when the rotating wave loses stability via Hopf bifurcation at $\alpha = 17.399$, and the fact that the homoclinic loop starts being attracting somewhere around $\alpha = 16.8$, combined with the above observation, could consistently be explained by a subcritical branch bifurcating off of the rotating wave. This subcritical torus would then provide both the missing basin of attraction boundary, and would cause the onset of attractivity of the homoclinic loop by colliding with it. This appears as a plausible explanation, but we have no numerical or analytical information in this direction available at the present time.

5b. The heteroclinic loop. We will now examine the saddle connection structure that persists between $\alpha = 16.00$, when the bimodal branch starts existing with two unstable eigenvectors, up to $\alpha = 16.1399$ (the value for which the unimodal and bimodal branches merge) when one of these eigenvectors becomes stable. Through this entire region the attractor is the rotating wave that bifurcated at 13.005, while the unimodal branch also exists possessing one unstable eigenvector.

Figure 5.3 shows a typical numerical experiment in this region ($\alpha = 16.1$). As in § 5a, we have two bimodal steady states u and u', but in this case each possesses two

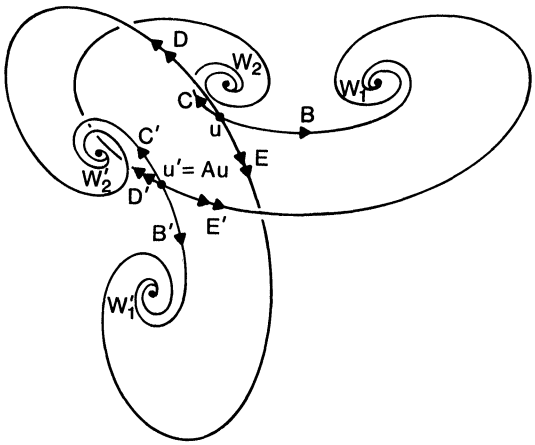

FIG. 5.3. *The bimodal steady state u has a two-dimensional unstable manifold (B, C, D, or E) and perturbations in the distinct four directions terminate in four distinct (W_1, W_2, W_1', W_2') unimodal steady states. A similar picture appears about $u' = Au$ with the notable exception that its weak unstable manifold (B', C') connects with the same fixed points (W_1' and W_2') as does the strong unstable manifold (D, E) of u. Likewise, the strong unstable manifold (D', E') of u' connects with the same fixed points (W_1 and W_2) as does the weak unstable manifold (B, C) of u.*

unstable eigenvectors. We will again follow numerically trajectories initialized approximately on these eigenvectors. The local approximation to the unstable submanifolds is again obtained by taking points B, C, D, and E on each side of each unstable eigendirection close to the bimodal saddle u. Points E and D lie on opposite sides of the strong unstable eigendirection (the one corresponding to the largest positive eigenvalue) while points B and C lie on the weak unstable eigendirection.

In addition, there exist four unimodal steady states, W_1, W_1', W_2, and W_2', each of them being a $\pi/2$ translation of the previous one (resulting from the action of $D(4)$). All unimodal waves are also unstable (saddles) but they possess one single unstable eigendirection. When the Galerkin-based integrator is used to follow the trajectories, we observe that the two that approximate the strong unstable submanifold of u (those starting at D and E) are attracted to the unimodal states W_2' and W_1', respectively. The two that approximate the weak unstable submanifold of u (starting at B and C) are attracted to the other two unimodal saddles W_1 and W_2. W_1 is a π-shift of W_2, and W_1' is a π-shift of W_2' (images under the action of $D(2)$). We observed that trajectories initialized at any nontrivial linear combination of the unstable eigenvectors were attracted by the rotating wave, which is stable through the entire region of interest. The FPT-integrator, initialized on any of the unstable eigendirections, would approach the corresponding unimodal saddle but would eventually burst away from it in the direction of its single unstable eigendirection and quickly approach the rotating wave.

Observations similar to the ones around point u were obtained around point u'. The only difference, which is crucial in what follows, was that the *strong* unstable submanifold of u' connected with the same unimodal saddles, W_1 and W_2, as did the *weak* unstable submanifold of u. On the other hand, the *weak* unstable submanifold of u' connected with W_1' and W_2', as did the *strong* unstable submanifold of u. This entire structure, connecting saddles between the unimodal and the bimodal branches, we call a persistent *heteroclinic* loop.

Let $u \in B$ be a bimodal steady state in R_1S_1 (see Fig. 5.4). Then so is Au. $dF(u)$ possesses two unstable eigenvectors $v_1 \in R_1S_2$ and $v_2 \in R_2S_2$. The unstable eigenvectors at Au are

$$Av_1 = AR_1S_2v_1 = R_2S_2Av_1 \in R_2S_2$$

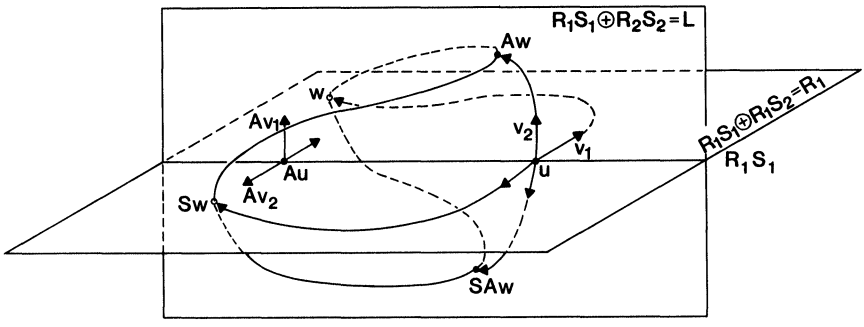

FIG. 5.4. *The bimodal steady state $u \in R_1S_1$ has two unstable directions, $v_1 \in R_1S_2$ and $v_2 \in R_2S_2$. Perturbations on opposite sides of the direction v_1 (v_2) lie in the invariant subspace $R_1S_1 \oplus R_1S_2 = R_1(R_1S_1 \oplus R_2S_2 = L)$ and terminate at the unimodal steady states $\{w, Sw\}$ ($\{Aw, SAw\}$) since the unstable directions of these states are normal to their invariant subspace $R_1(L)$.*

and

$$Av_2 = AR_2S_2v_2 = R_1S_2Av_2 \in R_1S_2.$$

Choose initial data $u + v_1 \in R_1S_1 \oplus R_1S_2 = R_1$. The solution remains in R_1, but now Av_2, the weak unstable eigendirection of Au lies in R_1S_2 and consequently Au is also a saddle in R_1S_2. Two more steady states are to be found in R_1S_2. They are the unimodal steady states w and Sw, where we recall that $Sw(x) = w(x+\pi)$, the π-shift of w. Now, the unstable eigenvector at w as well as at Sw is in $R_2 \perp R_1$, so that both appear as sinks in R_1. If, as the numerical evidence shows, the trajectory starting at $u + v_1$ terminates at w (say), then a trajectory starting on the opposite side $u - v_1$ of the strong stable manifold of u will be attracted to Sw.

Proof. $Su = SR_1S_1u = R_1S_1Su = R_1S_1u = u \quad (S_1S = S_1)$, but $Sv_1 = SR_1S_2v_1 = R_1SS_2v_1 = -R_1S_2v_1 = -v_1 \ (SS_2 = -S_2S)$. Thus, $u - v_1 = S(u + v_1)$ and since $SF(\omega) = F(S\omega)$ the solution to the initial value problem with initial data $u - v_1$ is equal to S times the solution of the initial value problem with initial data $u + v_1$ (i.e., its π-shift).

Similar arguments apply with initial data $u + v_2$ and $u - v_2$. The trajectory starting at $u + v_2$ remains in the invariant subspace L and is attracted by the unimodal state Aw while the trajectory starting at $u - v_2$ gets attracted to SAw.

We now examine what occurs when $D(4)$ acts on this entire structure (multiplication by A). Recall that L and R_1 are thus mapped into each other. $AF(\omega) = F(A\omega)$ and the fact that the unstable eigenvectors at Au are Av_1 and Av_2 indicate that the trajectories emanating from Au in these directions are simply A times the trajectories emanating from u. Because there are exactly two unimodal steady states in the subspace R_1 (w and Sw), the weak unstable submanifold of Au will be attracted by them. It is however, the strong unstable submanifold of u that lives in R_1 and is also attracted to them. The same considerations hold for the invariant subspace L, interchanging the roles of strong and weak unstable submanifolds and shifting the unimodal steady states by A (to Aw and SAw).

5c. Transition from heteroclinic to homoclinic. Since we know (§ 3c) that the unimodal and the bimodal branch will merge at $\alpha = 16.1399$, it is interesting to observe the implications of this bifurcation for the saddle connections we have described.

As we approach 16.1399 from below, the two unimodal states in R_1 approach the bimodal state whose weak unstable eigenvector lies in R_1, namely Au. At the same time, the two unimodal states in L approach the bimodal state whose weak unstable eigenvector lies in L, namely u. As the weak unstable eigenvalue of u (Au) crosses zero at 16.1399, the pair of unimodal states on L (R_1) collapse on the bimodal saddle u (Au). The strong unstable manifold of Au (u) which was attracted by the two unimodal states on L (R_1) now becomes attracted to u (Au) along its newborn stable eigendirection (see Fig. 5.5). This gives us a smooth transition from the heteroclinic loop to the left of 16.1399 to the homoclinic loop discussed in § 5a.

Numerical evidence indicates that neither the heteroclinic loop ($16 < \alpha < 16.1399$) nor the homoclinic loop immediately to the right of $\alpha = 16.1399$ are attracting. It is only around $\alpha = 16.8$ that the homoclinic loop becomes attracting, coexisting with the stable rotating wave.

For α smaller than (and sufficiently close to) 22.554 a Shilnikov box-type argument applies as long as the ratio of the single positive to the absolutely smallest negative eigenvalue is small enough. This guarantees the attractivity of the homoclinic loop. A "pulsing wave" orbit should approach the saddle-connections between u and Au, and

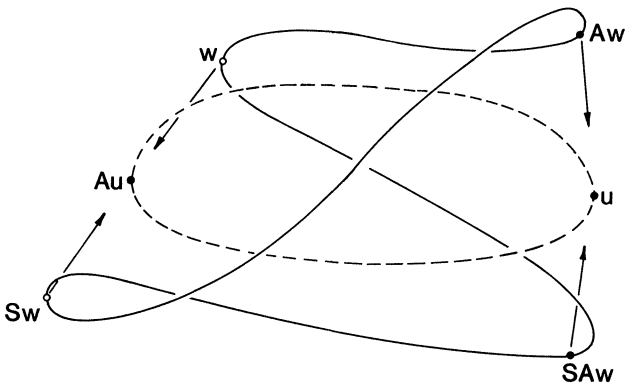

FIG. 5.5. *As α approaches* 16.1399, *the unimodal branch (solid line) merges with the bimodal branch (dotted line) in a two-to-one fashion. In particular, the two unimodal steady states $\{Aw, SAw\}$ ($\{w, Sw\}$) connected by the weak unstable manifold at $u(Au)$ collapse to u (Au) as the eigenvalue corresponding to this weak instability passes through zero.*

the transit times near these saddles should become increasingly longer. We have not observed this phenomenon numerically; it is possible that higher accuracy simulations are necessary.

Even when these loops are unstable, however, they do affect the transients in their neighborhood. In particular, the scaling properties we have discussed in § 3b imply that scaled replicas of these dynamics will occur repeatedly as α increases, and we expect them to play an important role in the increased complexity of the dynamics of the full K-S observed at high values of α. For α less than 16.1399 the heteroclinic loop illustrates the tendency of the system to channel bimodal behavior down into unimodal behavior, while after 16.1399 bimodal behavior prevails. This is in agreement with the increase in the dimension of the global attractor predicted by the theory of inertial manifolds for the K-S (Nicolaenko, Scheurer, and Temam 1985). This theory applied to the K-S provides both a proof of the low-dimensional nature of the dynamic behavior of the K-S equation and estimates of the dimension of the global attractor.

Our detailed study of the bifurcations of the K-S may be considered as a corroboration of these results. Furthermore, the structures we locate must live on the universal attractor. In the case of PDEs possessing a Lyapunov functional it has been shown (Babin and Vishik, (1987)) that this universal attractor is the closure of the unstable manifolds of normal hyperbolic fixed points. It is therefore possible that detailed knowledge of the various stable and unstable, fixed and time-dependent K-S solutions along with their unstable manifolds may play an important role in the location and characterization of the universal attractor. One might even expect that the bifurcations of these solutions may be connected with the jumps in the dimension of the inertial manifold as α grows. We consider this potential connection between bifurcation theory and inertial manifold theory an exciting direction for further research.

6. Conclusions. The low-dimensional behavior of the K-S has been corroborated by numerical and analytical work on its bifurcations for low values of the parameter α (Fig. 6.1 depicts the steady state bifurcation diagram up to $\alpha = 70$). The symmetries inherent in the equation give rise to structurally stable saddle connections that would otherwise be unstable. Tracking unstable, saddle-type solutions and their unstable manifolds was instrumental in understanding the observable dynamics and in suggesting otherwise unapparent directions for analytical work. In this fashion, a numerical scheme respecting the symmetries of the problem proved valuable in detecting saddle-point connections.

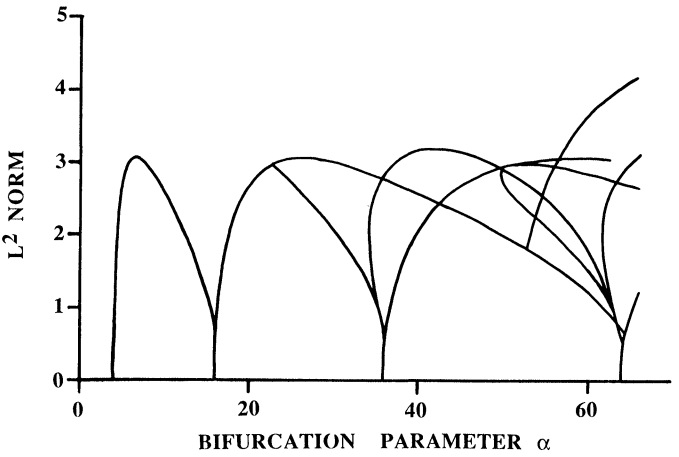

FIG. 6.1. *Steady state bifurcation diagram extending to* $\alpha = 70$.

Acknowledgments. The authors would like to thank M. Golubitsky for his valuable comments, as well as the referee for suggesting the center manifold approach to the bifurcation theorem for the traveling wave.

Note added in proof. Since this manuscript was first submitted, a number of publications on the subject have appeared. We consider the following particularly relevant:

J. M. GREEN AND J.-S. KIM (1988), *The steady states of the Kuramoto-Sivashinsky equation*, Physica D, 33, pp. 99-120.

D. ARMBRUSTER, J. GUCKENHEIMER, AND P. J. HOLMES (1988), *Heteroclinic cycles and modulated travelling waves in systems with O(2) symmetry*, Physica D, 29, pp. 257-282.

——— (1989), *Kuramoto-Sivashinsky dynamics on the center-unstable manifold*, SIAM J. Appl. Math., 49, pp. 676-691.

REFERENCES

S. V. ALEKSEENKO, V. YE. NAKORYAKOV, AND B. G. POKUSAEV (1985), *Wave formation on a vertical falling liquid film*, AIChE J., 31, pp. 1446-1460.

——— (1985), *Wave formation on vertical falling liquid films*, Int. J. Multiphase Flow, 11, pp. 607-627.

N. AUBRY, P. HOLMES, J. LUMLEY, AND E. STONE (1986), *Dynamical System/Coherent Structure Approach to the Fully Developed Wall Layer*, Cornell University Report, Ithaca, NY.

A. V. BABIN AND M. I. VISHIK (1983), *Regular attractors and semi-groups of evolution equations*, J. Math. Pures Appl., 62, pp. 441-491.

D. J. BENNEY (1966), *Long waves on liquid films*, J. Math. & Phys., 45, pp. 150-155.

M. S. BERGER (1977), *Nonlinearity and Functional Analysis*, Academic Press, New York.

H.-C. CHANG (1986a), *Nonlinear waves on liquid film surfaces*—I. Flooding in a vertical tube, Chem. Eng. Sci., 41, pp. 2463-2476.

——— (1986b), Travelling waves on fluid interfaces: normal form analysis of the Kuramoto-Sivashinsky equation, Phys. Fluids, 29, pp. 3142-3147.

L.-H. CHEN AND H.-C. CHANG (1986), *Nonlinear waves on thin film surfaces—II. Bifurcation analyses of the long-wave equation*, Chem. Eng. Sci., 41, pp. 2477-2486.

P. CHOSSAT (1985), *Interaction of rotating waves in the Çouette-Taylor problem*, Proc. Acad. Sci. Paris I(8), pp. 251-255.

P. CHOSSAT AND G. IOOSS (1985), *Primary and secondary bifurcations in the Couette-Taylor problem*, Japan J. Appl. Math., 2, pp. 37-68.

B. I. COHEN, J. A. KROMMES, W. M. TANG, AND M. N. ROSENBLUTH (1976), *Non-linear saturation of the dissipative trapped-ion mode by mode-coupling*, Nucl. Fusion, 16, pp. 971-992.

G. DANGELMAYR AND D. ARMBRUSTER (1986), *Steady state mode interactions in the presence of O(2) symmetry and in non-flux boundary value problems*, Contemp. Math., 56, pp. 53-68.

E. J. DOEDEL (1981), AUTO: *a program for the bifurcation analysis of autonomous systems*, Congr. Numer., 30, pp. 265-284.

J. C. EILBECK (1986), *The pseudo-spectral method and path following in reaction diffusion bifurcation studies*, SIAM J. Sci. Stat. Comp., 7, pp. 599-610.

——— (1987), *Numerical studies of bifurcation in reaction-diffusion models using pseudo-spectral and path-following methods*, in Bifurcation: Analysis, Algorithms and Applications, T. Kuepper, R. Seydel, and H. Troger, eds., Birkhaeuser, Basel.

S. FAUVE (1985), *Large scale instabilities in cellular flows*, preprint, Woods Hole Summer Program.

C. FOIAS, B. NICOLAENKO, G. R. SELL, AND R. TÉMAM (1988), *Inertial manifolds for the Kuramoto-Sivashinsky equation and estimates of their dimension*, J. Math. Pures et Appl., 67, pp. 197-226.

U. FRISCH, Z. S. SHE, AND O. THUAL (1986), *Viscoelastic behavior of cellular solutions to the Kuramoto-Sivashinsky model*, J. Fluid Mech., 168, pp. 221-240.

M. GOLUBITSKY AND D. G. SCHAEFFER (1985), *Singularities and Groups in Bifurcation Theory*, Vol. 1, Springer Verlag, NY.

J. GUCKENHEIMER (1986), *A codimension two bifurcation with circular symmetry*, Contemp. Math., 56, pp. 175-184.

J. GUCKENHEIMER AND P. HOLMES (1986), *Structurally stable heteroclinic cycles*, preprint, Ithaca, NY.

A. P. HOOPER AND R. GRIMSHAW (1985), *Nonlinear instability at the interface between two viscous fluids*, Phys. Fluids, 28, pp. 37-45.

J. M. HYMAN AND B. NICOLAENKO (1986), *The Kuramoto-Sivashinsky equation: a bridge between PDEs and dynamical systems*, Physica, 18D, pp. 113-126.

——— (1987), *Coherence and chaos in the Kuramoto-Velarde equation*, in Directions in Partial Differential Equations, Academic Press, New York.

J. M. HYMAN, B. NICOLAENKO, AND S. ZALESKI (1985), *Order and complexity in the Kuramoto-Sivashinsky model of weakly turbulent interfaces*, Physica, 23D, pp. 265-292.

G. IOOSS (1984), *Bifurcations and transitions to turbulence in hydrodynamics*, CIME Session on Bifurcation Theory and Applications, L. Salvadori, ed., Lect. Notes in Math. 1057, Springer-Verlag, New York, pp. 152-200.

Y. KURAMOTO AND T. TSUZUKI (1976), *Persistent propagation of concentration waves in dissipative media far from thermal equilibrium*, Progr. Theoret. Phys., 55, pp. 365-369.

Y. C. LEE AND H. H. CHEN (1982), *Nonlinear dynamical models of plasma turbulence*, Phys. Scripta, (Sweden), T2, pp. 41-47.

S. P. LIN (1974), *Finite-amplitude side-band stability of a viscous film*, J. Fluid Mech., 63, pp. 417-429.

D. M. MICHELSON (1985), *Steady solutions of the Kuramoto-Sivashinsky equation*, Physica, 19D, pp. 89-111.

D. M. MICHELSON AND G. I. SIVASHINSKY (1977), *Nonlinear analysis of hydrodynamic instability in laminar flames—II. Numerical experiments*, Acta Astr., 4, pp. 1207-1221.

A. A. NEPOMNYASHCHII (1973), *Stability of wavy conditions in a film flowing down an inclined plane*, translated from Izv. AN SSSR Mekh. Zhid. i Gaza, 3, pp. 28-34.

B. NICOLAENKO, B. SCHEURER, AND R. TÉMAM (1985), *Some global dynamical properties of the Kuramoto-Sivashinsky equations: nonlinear stability and attractors*, Physica, 16D, pp. 155-183.

G. I. SIVASHINSKY (1977), *Nonlinear analysis of hydrodynamic instability in laminar flames—I. Derivation of basic equations*, Acta Astr., 4, pp. 1177-1206.

T. SHLANG AND G. I. SIVASHINSKY (1982), *Irregular flow of a liquid film down a vertical column*, J. Phys., 43, pp. 459-466.

O. THUAL, U. FRISCH, AND M. HÉNON (1986), *Application of polar decomposition to an equation governing the dynamics of wrinkled flame fronts*, preprint.

O. YU. TSVELODUB (1980), *Stationary travelling waves on a film flowing down an inclined plane*, translated from Izv. AN SSSR Mekh. Zhid. i Gaza, 4, pp. 142-146.